

1 **Using large eddy simulations to reveal the size, strength, and**
2 **phase of updraft and downdraft cores of an Arctic mixed phase**
3 **stratocumulus cloud**

4 **Erika L. Roesler¹, Derek J. Posselt², Richard B. Rood³**

5 ¹Sandia National Laboratories, Albuquerque, New Mexico, USA

6 ²Jet Propulsion Laboratory, Pasadena, California, USA

7 ³University of Michigan, Ann Arbor, Ann Arbor, Michigan, USA

8 **Key Points:**

- 9 • Two subgrid-scale turbulence schemes, 1.5-TKE and CLUBB, were compared in sim-
10 ulations of an Arctic mixed-phase stratocumulus cloud.
- 11 • Comparing to observations show both schemes produce the liquid water profiles within
12 measurement variability but not ice water profiles.
- 13 • Updraft and downdraft cores are different in size, similar in strength, and composed of
14 both liquid and ice.

This is the author manuscript accepted for publication and has undergone full peer review but has not been through the copyediting, typesetting, pagination and proofreading process, which

**Corresponding author: E. L. Roesler, eroesler@gmail.com
may lead to differences between this version and the Version of Record. Please cite this article as doi: [10.1002/2016JD026055](https://doi.org/10.1002/2016JD026055)**

Abstract

Three-dimensional large eddy simulations (LES) are used to analyze a springtime Arctic mixed-phase stratocumulus observed on 26 April 2008 during the Indirect and Semi-Direct Aerosol Campaign (ISDAC). Two subgrid-scale turbulence parameterizations are compared. The first scheme is a 1.5-order turbulent kinetic energy (1.5-TKE) parameterization that has been previously applied to boundary layer cloud simulations. The second scheme, Cloud Layers Unified By Binormals (CLUBB), provides higher-order turbulent closure with scale-awareness. The simulations, in comparisons with observations, show that both schemes produce the liquid profiles within measurement variability, but underpredict ice water mass and overpredict ice number concentration. The simulation using CLUBB underpredicted liquid water path more than the simulation using the 1.5-TKE scheme, so the turbulent length scale and horizontal grid box size were increased to increase liquid water path and reduce dissipative energy. The LES simulations show this stratocumulus cloud to maintain a closed cellular structure, similar to observations. The updraft and downdraft cores self-organize into a larger meso- γ scale convective pattern with the 1.5-TKE scheme, but the cores remain more isotropic with the CLUBB scheme. Additionally, the cores are often composed of liquid and ice instead of exclusively containing one or the other. These results provide insight into traditionally unresolved and unmeasurable aspects of an Arctic mixed-phase cloud. From analysis, this cloud's updraft and downdraft cores appear smaller than other closed-cell stratocumulus such as midlatitude stratocumulus and Arctic autumnal mixed-phase stratocumulus due to the weaker downdrafts and lower precipitation rates.

1 Introduction

The areal extent of Arctic sea ice and its rapid decline during the past decade have climatological significance beyond the Arctic [Stroeve *et al.*, 2012]. For example, a connection could exist between the loss of Arctic ice and midlatitude weather patterns [Francis and Vavrus, 2012]. Elements of the Arctic environment that can contribute to further sea ice melt include boundary-layer stratocumulus clouds. These types of clouds are common in the Arctic and are mostly mixed phase, meaning they can contain both liquid and ice particles. Because of the ubiquitous nature of these liquid-containing clouds in the Arctic, they have a net positive radiative forcing, warming the surface through most of the year [Curry *et al.*, 1996; Intrieri *et al.*, 2002].

46 How these mixed-phase clouds persist despite the coexistence of ice and liquid within
47 the cloud is an active scientific question. It is known that these mixed-phase boundary layer
48 clouds contain liquid water at the top of the cloud. Longwave cooling from this liquid layer
49 leads to negative buoyancy, which drives parcels downward into the cloud. There could also
50 be ice precipitation from the cloud. Within the updraft and downdraft cores, it is believed that
51 ice and liquid water compete to be the dominant phase. Through this paper, we present our
52 findings regarding the properties of the cores in mixed-phase clouds in order to better under-
53 stand their persistence and longevity.

54 Several Arctic field campaigns have been conducted during the last decade with goals
55 to obtain statistical properties and insight into the large-scale and internal dynamics involved
56 with mixed-phase clouds' formation, persistence, and decay. For instance, during the SHEBA
57 (Surface Heat Budget of the Arctic) campaign which occurred in the years 1997 - 1998, surface-
58 based remote sensors were used for year-long measurements [Shupe *et al.*, 2005a]. It was re-
59 ported that multi-layered cloud scenes with all-liquid, all-ice, or mixed-phase clouds were com-
60 mon, and that mixed-phase clouds had a higher likelihood of occurring during the transition
61 seasons of spring and autumn. During SHEBA, all-liquid clouds were observed to occur dur-
62 ing about 20% of the year, and mixed-phase were observed to occur about 40% of year [Shupe
63 *et al.*, 2005a].

64 Properties of single-layer mixed-phase stratocumulus clouds were measured during the
65 MPACE (Mixed-Phase Arctic Clouds Experiment) [McFarquhar *et al.*, 2007] field campaign
66 and the SEARCH (Study of Environmental Arctic Change) long-term measurements in far-
67 northern Canada [Eicken, 2013]. It was found that throughout the cloud's height, the liquid-
68 to-ice ratio did not always linearly decrease as cloud temperature decreased. Water in its liq-
69 uid state could exist at temperatures as low as -31° C [McFarquhar *et al.*, 2007; de Boer *et al.*,
70 2009]. During the Arctic Summer Cloud Ocean Study (ASCOS) conducted in summer 2008,
71 Shupe *et al.* [2013] showed that most of the observed stratocumulus clouds were decoupled
72 from the surface, meaning surface fluxes were not driving turbulent motion within the cloud.

73 The ISDAC (Indirect and Semi-Direct Aerosol Campaign) field campaign conducted in
74 April 2008 made measurements of boundary-layer clouds during a time of the year when de-
75 coupled boundary layer clouds were likely to be observed. Springtime in the Arctic is prior
76 to the onset of extensive and rapid sea ice melt, so surface energy fluxes are usually low from
77 the ocean to the atmosphere. ISDAC was based out of the long-term monitoring DOE ARM

(Department of Energy Atmospheric Radiation Measurement) program field site located near Barrow, Alaska on the North Slope of Alaska. Mixed-phase clouds were previously observed at this location during other campaigns such as SHEBA, MPACE, and FIRE-ACE (First International Satellite Cloud Climatology Project Regional Experiment - Arctic Clouds Experiment) [Barrie, 1986; Ghan *et al.*, 2007; Shupe *et al.*, 2005b, 2006]. Single-layer mixed-phase stratocumulus clouds were observed on April 8 and April 26.

The focus of this study is the springtime Arctic stratocumulus cloud that occurred on April 26, 2008. In previous numerical studies of this mixed-phase cloud, Ovchinnikov *et al.* [2011] found the stability and longevity of this mixed-phase cloud was sensitive to the prescribed ice concentration, where too little or too much prescribed ice caused an all-liquid cloud or depleted most of the condensate. It was also found that the stability of the springtime mixed-phase clouds and their turbulent kinetic energy production relies on longwave cooling at the cloud top and the continuous growth of ice particles in the downdrafts. Ovchinnikov *et al.* [2011] and Morrison *et al.* [2012] showed that a precarious relationship exists between the microphysics, turbulence, and other environment components that can either drive the cloud into a stable state, lead to its dissipation, or prevent its formation.

Given the work that has been done investigating the microphysics and the liquid-to-ice ratios of this cloud, we provide further analysis regarding the cores of this mixed-phase cloud with three-dimensional (3D) large-eddy simulations (LES). LES simulations have the ability to resolve vertical motion of the largest eddies of the boundary layer circulation (definition from Cheng *et al.* [2010]) of meso- γ scale cloud organization.¹ Two types of turbulent kinetic energy closures are used in this assessment. The first scheme is a 1.5-order turbulent kinetic energy (called 1.5-TKE hereafter) parameterization developed by Deardorff [1980]. The 1.5-TKE scheme was developed for simulations that can resolve the turbulent motion of stratocumulus clouds. The second scheme, Cloud Layers Unified By Binormals (CLUBB), is a higher-order closure model that closes the second- and third-order terms of the Reynolds-Averaged Navier Stokes (RANS) equations via the use of probability distribution functions. A thorough description of CLUBB is given by Golaz *et al.* [2002] and Larson *et al.* [2002]. CLUBB is designed to operate in a consistent manner in many environments and for many types of clouds including boundary layer cloud systems (e.g. Golaz *et al.* [2002], Larson *et al.* [2012], Bogen-schutz *et al.* [2013]). However, CLUBB has not been tested at LES scales for an Arctic mixed-

¹ The meso- γ scale is defined as being 2-20 kilometer in size with a 3-30 min timescales from Orlandi [1975].

109 phase stratocumulus cloud. We recognize that CLUBB was not intended to be used at these
110 resolutions, but there is a community need to understand the performance of scale-aware pa-
111 rameterizations in many environments. This paper, therefore, uses CLUBB at LES scales to
112 better understand the updraft and downdraft cores of an Arctic mixed-phase cloud.

113 This paper aims to answer the following questions:

- 114 1. What are the macrophysical differences of the cloud when different subgrid turbulent
115 parameterizations are used?
- 116 2. What are the properties (i.e., size, strength, phase) of the updraft and downdraft cores
117 of this mixed phase cloud?
- 118 3. How do these properties compare with current knowledge of other stratocumulus cloud
119 cores?

120 To answer these questions, the paper is organized as follows. In Section 2, an overview
121 of the turbulent closure schemes is given. Section 3 contains the observational description of
122 the mixed-phase cloud and the model configuration. Section 4 compares the control-run sim-
123 ulations with observations. Section 5 compares the mixed-phase clouds produced by the two
124 turbulence schemes, and Section 6 shows how modifications to CLUBB's scheme changes macro-
125 scopic properties of the mixed-phase cloud through its computed turbulent kinetic energy. Sec-
126 tion 7 presents the sizes, strengths, and phase in the updraft and downdraft cores and com-
127 pares these findings to current knowledge of other stratocumulus clouds. The summary and
128 conclusions section follows.

129 **2 Model Description**

130 We use SAM (System for Atmospheric Modeling, version 6.8.2) [*Khairoutdinov and Ran-*
131 *dall, 2003*], a model capable of running in large eddy simulation (LES) or cloud resolving model
132 (CRM) configurations, for this study. *Khairoutdinov and Randall [2003]* contains a thorough
133 description of SAM. In SAM, we use the Morrison two-moment microphysics scheme, which
134 predicts the mass and concentration of drops, ice, rain, snow, and graupel [*Morrison et al., 2005*].
135 The radiation package is based on the radiation scheme from the NCAR Community Atmo-
136 sphere Model (CAM, version 3.0) [*Collins et al., 2006*]. In SAM, anelastic momentum equa-
137 tions are advanced in time for the resolved wind components, the liquid/ice water static en-
138 ergy, and the total nonprecipitating and precipitating water mixing ratios in Cartesian coor-

139 dinates. Higher-order moments resulting from the filtered Navier-Stokes equations need clo-
 140 sure by a subgrid-scale scheme. Two subgrid-scale turbulence parameterizations, CLUBB ver-
 141 sion 1.18 and the 1.5-TKE parameterization, are used for closure in SAM.

142 *Deardorff* [1980]’s 1.5-TKE turbulence scheme is a three-dimensional turbulence model
 143 for stratocumulus-capped mixed layers where the subgrid-scale terms are closed with a gradient-
 144 diffusion closures. An example of this closure for buoyancy flux would be $\overline{w'\theta'_l} = -K_h \partial\overline{\theta}_l/\partial z$,
 145 where K_h is the subgrid eddy coefficient for scalar quantities given by $(1+2l/\Delta s) K_m$, K_m
 146 is the subgrid-scale eddy coefficient for momentum given by $0.10 l \overline{E}^{1/2}$, l is the subgrid-scale
 147 mixing length, and $\overline{E}^{1/2}$ is the subgrid scale kinetic energy. The kinetic energy is given by
 148 $\overline{E} = \frac{1}{2}(\overline{u'^2} + \overline{v'^2} + \overline{w'^2})$. The subgrid-scale mixing length, l , is set to not exceed the grid
 149 scale, $\Delta s = (\Delta x \cdot \Delta y \cdot \Delta z)^{1/3}$, in magnitude. Additional restrictions are placed on the mag-
 150 nitude of the mixing length scale for regions of positive or negative buoyancy [*Deardorff*, 1980].

151 CLUBB has prognostic equations for the second-order terms and closes third-order terms
 152 using probability distribution functions from a pre-selected family of double Gaussian prob-
 153 ability distribution functions. The moments or correlations of the variables are computed by
 154 integrating over the probability distribution function. The family of probability distribution func-
 155 tions are chosen to be Gaussian and quasi-normal so that odd-ordered moments do not van-
 156 ish [*Golaz et al.*, 2002; *Larson et al.*, 2002]. Because the probability distribution function is
 157 from the double Gaussian family, the solution is analytic and an equation consisting of the prod-
 158 uct of the widths, locations, and mean values of the variables is produced. The probability dis-
 159 tribution function thus closes the higher order moments, which are then used to advance the
 160 prognostic equations.

161 This version of CLUBB closes the second-order horizontal winds, $\overline{u'w'}$ and $\overline{v'w'}$, with
 162 a gradient-diffusion approach, i.e., $\overline{u'w'} = -K_m \partial\overline{u}/\partial z$ and $\overline{v'w'} = -K_m \partial\overline{v}/\partial z$, where
 163 $K_m = c_k L_1 \overline{e}^{1/2}$, $c_k = 0.548$, L_1 is an eddy length scale, and \overline{e} is the subgrid-scale turbulent
 164 kinetic energy [*Golaz et al.*, 2002]. The kinetic energy is also given by $\overline{e} = \frac{1}{2}(\overline{u'^2} + \overline{v'^2} +$
 165 $\overline{w'^2})$. Dissipation terms are contained in the second- and third-order prognostic equations. Each
 166 of these dissipation terms is also a function of an eddy length scale [*Golaz et al.*, 2002; *Lar-*
 167 *son et al.*, 2012]. The eddy length scale is calculated from the idea that given a parcel’s buoy-
 168 ancy within the vertical column, the parcel’s vertical displacement is based on its initial ki-
 169 netic energy. Limits are set on the length scale to maintain numerical stability, and the default
 170 maximum value of the length scale in CLUBB is one-fourth of the grid size [*Larson et al.*, 2012].

171 Latent heat release from ice formation is not explicitly taken into account in this version of
172 CLUBB, and ice and precipitation processes are handled in the microphysics. More recent de-
173 velopment work addresses ice mass in CLUBB. See, for example, *Storer et al.* [2015]. This
174 treatment of ice and precipitation is consistent between the 1.5-TKE and CLUBB schemes.
175 Table 1 lists prognostic variables of the CLUBB and the 1.5-TKE scheme from the filtered
176 Navier-Stokes equations.

177 **3 Description of the Mixed-Phase Cloud and Model Configuration**

178 On April 26, 2008, a single-layered mixed phase cloud system was observed near Bar-
179 row, Alaska. A region of high pressure centered over the Arctic Ocean and weak easterly wind-
180 flow was observed at Barrow, Alaska and pushed a cloud system towards Barrow. The ocean
181 was mostly ice-covered at this time [*McFarquhar et al.*, 2011]. Reanalysis products from ERA-
182 40 Interim during 25-26 of April, 2008 show low-level cloudiness off the coast near Barrow
183 [*European Centre for Medium-Range Weather Forecasts*, 2009]. Figure 1 shows a snapshot of
184 the computed fractional cloud cover from the reanalysis product on 26 April 2008 at 06:00
185 GMT at ~ 865 hPa. The cloud, as depicted by the reanalysis, appears on 25 April in the Chukchi
186 Sea between the Russian and Alaskan landmasses. The reanalysis shows the cloud layer to be
187 mostly between 800 and 900 hPa during the 25-26 of April, 2008 advecting westward, and
188 eventually covering the North Slope. Reports from observations differ slightly. On 26 April
189 2008, the mixed-phase cloud was actually several hundred kilometers from Barrow over the
190 ocean when in situ aircraft measurements were taken. We thus rely on a combination of in-
191 formation from reanalysis and in situ aircraft measurements to simulate an idealized represen-
192 tation of this Arctic mixed-phase cloud. The aircraft measurements are mainly used to initial-
193 ize and constrain the microphysics of the LES simulations and the reanalysis is mainly used
194 for the dynamics initial conditions.

195 The boundary and initial conditions for SAM's surface fluxes, temperature profile, and
196 wind profiles are taken from the DOE ARM site's radar and atmospheric sounding measure-
197 ments and from the 26 April 2008 aircraft observations. Atmospheric profiles are derived us-
198 ing constrained variational analysis based on ECMWF analysis fields [*Zhang and Lin*, 1997;
199 *Zhang et al.*, 2001; *Xie et al.*, 2006]. This technique uses sounding measurements of winds,
200 temperature, and water vapor mixing ratio to interpolate GCM grid-scale vertical velocity and
201 advective tendencies. The profiles are smoothed to remove noise.

202 The resultant idealized profiles are shown in Figure 2. The temperature and moisture pro-
203 files in the lower troposphere were modified to more closely match the structure of the bound-
204 ary layer at the time and location of the flight. In Figure 2a, the temperature at the surface is
205 265.3° K and decreases to 256.7° K at 900 m, then begins to increase with height to form
206 a temperature inversion. The water vapor is well-mixed in the boundary layer from the sur-
207 face to 900 m (Figure 2b). When the cloud is initially formed in SAM, the increasing tem-
208 perature and decreasing water vapor with height above 900 m creates a vertically stable at-
209 mosphere. Figures 2c, 2d, and 2e show the horizontal and vertical wind profiles of the large-
210 scale flow. The time tendencies of these winds are used to advect the cloud in the LES do-
211 main. The simulations are nudged to large-scale winds every 4 hours. The temperature and
212 water vapor mixing ratio are not nudged.

213 The simulation is run for 24 hours on a three-dimensional, doubly-periodic domain with
214 $120 \times 120 \times 120$ grid points centered at 71.32° North, -156.61° West. A uniform vertical grid
215 is used with grid spacings of $\Delta z = 20$ m starting 20 m above the surface. The horizontal grid
216 spacings are $\Delta x = \Delta y = 100$ m, and the dynamical and radiation time steps are 2 seconds.
217 The grid spacing and time step were chosen so that numerical stability conditions are satis-
218 fied. This configuration defines the control run.

219 The aerosol size distribution parameters and composition in the cloud microphysical pa-
220 rameterization are prescribed in SAM. The aerosol size distribution mean diameter, D , geo-
221 metric standard deviation, σ_g , and initial aerosol number concentration, N_A , are initialized as
222 $D = 0.194 \mu\text{m}$, $\sigma_g = 1.48$, and $N_A = 199 \text{ cm}^{-3}$. These parameters are based on mea-
223 surements obtained during April 26, 2008 research flights [Ghan, 2010] and compiled by Pe-
224 ter Liu and Mike Earle. Measurements collected during the ISDAC campaign showed the pri-
225 mary aerosol composition to be sulfate mixed with organics, biomass burning, and sea salt [Mc-
226 Farquhar et al., 2011]. Zelenyuk et al. [2010] found that most of the larger particles over 0.1
227 μm in diameter were activated in the cloud, and that particle size was the most important pa-
228 rameter for aerosol activation, with sulfate content being of secondary importance. Based on
229 this information, the aerosol composition in SAM is set to be ammonium sulfate, $(\text{NH}_4)_2\text{SO}_4$,
230 with no insoluble, organic, or sea salt components. A comprehensive study of how aerosol con-
231 centration, composition, and size affect cloud droplet number has shown that approximating
232 the aerosol composition as the three-ion ammonium sulfate instead of more complicated molecule
233 is not expected to change the droplet number within the modeled cloud significantly [Roesler
234 and Penner, 2010]. A log-normal aerosol size distribution is used to compute the cloud con-

235 condensation nuclei (CCN) spectra for the Morrison microphysics, and droplet number concen-
 236 tration is predicted using the aerosol activation parameterization of *Abdul-Razzak and Ghan*
 237 [2000].

238 The ice nucleation is prescribed following the procedure in *Morrison et al.* [2011], *Ovchin-*
 239 *nikov et al.* [2011], and *Ovchinnikov et al.* [2014], which eliminates uncertainty in the nucle-
 240 ation mechanism. The ice nucleation is essentially nudged to a prescribed value under spe-
 241 cific environmental thresholds of supersaturation and liquid water concentration. The rate is
 242 given by

$$\begin{aligned}
 \frac{\partial N_i}{\partial t} &= \max\left(0, \frac{N_{i0} - N_i}{\Delta t}\right), & S_i \geq 0.05 \text{ or } q_l \geq 0.001 \text{ g kg}^{-1} \\
 \frac{\partial N_i}{\partial t} &= 0, & S_i < 0.05 \text{ or } q_l < 0.001 \text{ g kg}^{-1}
 \end{aligned}
 \tag{1}$$

246 where N_{i0} is the prescribed ice particle concentration, N_i is the model's predicted ice
 247 concentration computed after other species' tendencies have been computed in the previous
 248 time step, Δt is the model time step, S_i is the fractional supersaturation over ice, and q_l is the
 249 liquid water mixing ratio. N_{i0} is set to 0.5 L^{-1} . The sensitivity of the cloud's macrophysi-
 250 cal properties to initial ice concentration was tested by doubling N_{i0} to 1.0 L^{-1} and also re-
 251 ducing N_{i0} to 0.1 L^{-1} , similar to the work of *Ovchinnikov et al.* [2011]. The doubling of N_{i0}
 252 to 1.0 L^{-1} causes the ice water path to increase at the expense of the liquid water path. The
 253 reduction of N_{i0} to 0.1 L^{-1} causes the ice water content to be significantly smaller than what
 254 was observed. The cloud's response to changes in prescribed ice concentration are consistent
 255 with *Ovchinnikov et al.* [2011], who also tested ranges of N_{i0} . To maintain macrophysical fea-
 256 tures of a mixed-phased stratocumulus cloud with non-zero liquid and ice water paths, we de-
 257 termine that $N_{i0} = 0.5 \text{ L}^{-1}$ to be the best value for prescribed ice concentration. Compar-
 258 ison of N_{i0} to in-cloud observations occurs in Section 4.

259 The control run simulation of the Arctic mixed-phase cloud starts at GMT 117.5 and runs
 260 for 24 hours until 118.5 GMT. The first four hours are considered spin-up time in which the
 261 turbulence, liquid water path, and ice water path are developed in the LES domain. An ex-
 262 ample of this spin-up time is shown in Figure 3, where a cross-section of the three-dimensional
 263 vertical velocity is shown at $y = 6000 \text{ m}$ at 2 and 4 hours into the simulation with the 1.5
 264 TKE scheme. At 2 hours into the simulation, the updraft and downdraft cores have not de-

265 veloped throughout the domain. At 4 hours, the updraft and downdraft cores extend through-
266 out the domain and both liquid and ice are present (shown later).

267 **4 Control-Run Simulations Compared with Observations**

268 We next compare properties of the cloud from the simulations with the observations. We
269 emphasize at the outset that the goal is not to replicate the observed cloud. Instead, we aim
270 to simulate a persistent liquid-topped mixed phase cloud and highlight differences between the
271 real cloud and the simulations upon which it is based. This also documents the simulated clouds'
272 sensitivity to changes in the turbulence representation.

273 Profiles of the cloud's domain-averaged liquid number concentrations, ice number con-
274 centrations, liquid water mass mixing ratio, and ice water mass mixing ratio are compared with
275 ISDAC aircraft measurements in Figure 4. Measurements of the cloud micro- and macrophys-
276 ical properties were obtained from a 100 km aircraft flight leg within the cloud. The flight num-
277 ber was 31 (see www.acrf-campaign.arm.gov/idsac/flighttable.pdf), and the total aircraft flight
278 time was about 4 hours in duration. The measurements used here are when the aircraft por-
279 poised and flew in constant-altitude legs between 250 m and 1000 m above the surface. This
280 data was then binned by altitude into 20 m increments. The aircraft measurements showed most
281 of the liquid to be contained between 600 to 900 m. Ice was measured in the cloud from 380
282 m to 900 m, and it is estimated that small particles (low mass, high number) were between
283 700 m to 800 m and larger particles (high mass, low number) were between 400 m to 700 m.

284 Both the CLUBB and 1.5-TKE schemes reproduce a maximum in liquid water mass mix-
285 ing ratio near 800 m. The 1.5-TKE scheme over-predicts the liquid mass while the CLUBB
286 scheme under-predicts the liquid mass compared to the observations. The liquid number con-
287 centration maxima is better represented by both schemes than the mass mixing ratio. An in-
288 crease in liquid number and mass concentration was measured by the aircraft at 380 m, and
289 neither scheme reproduces this feature. The model's ice number concentration is at least twice
290 as much as was measured, and both schemes have less ice water mass mixing ratio by nearly
291 an order-of-magnitude.

292 Constraining ice crystal concentration has been a method of bringing the numerical cloud
293 microphysics closer to the measured values. It could be inferred from Figure 4d that choos-
294 ing $N_{i0} = 0.1 L^{-1}$ would bring the ice number concentration in the simulations closer to
295 the measurements. However, recall (from Section 3) that this causes the liquid water to increase

296 and the ice water to decrease causing the cloud to be mostly all-liquid. The modeled cloud
297 has the most macrophysical similarity to the measured cloud with the value of $N_{i0} = 0.5$
298 L^{-1} . We tested the variance and mean radius of the modified gamma distribution to exclude
299 the high concentration, low mass cloud particles. This was found to have little effect on the
300 ice number concentration and ice mass mixing ratio, suggesting additional work is needed to
301 fit this microphysics scheme to this mixed-phased cloud's liquid and ice concentrations.

302 Differences between measured and simulated ice water and liquid water are not uncom-
303 mon in high and low resolution simulations of mixed-phase clouds. *Avramov and Harrington*
304 [2010] and *Avramov et al.* [2011] had similar results of underpredicting ice water path using
305 a two-moment microphysics scheme and a bin microphysics scheme with a Smagorinsky-type
306 closure scheme for turbulence, respectively. *Solomon et al.* [2011] used a nested simulation of
307 the WRF model using bulk microphysics and a non-local-K closure scheme and also under-
308 predicted ice water path. Conversely, in a model intercomparison with single column models
309 and cloud resolving models of mixed-phase clouds in the fall, the ice water path was better
310 matched to observations than the liquid water path [*Klein et al.*, 2009]. Other simulations have
311 brought closer agreements between measurements and models for all phases of water in mixed
312 phase clouds through the use of spectral bin microphysics as shown by *Fan et al.* [2009] or
313 adaptive habit models (e.g. *Sulia et al.* [2014]).

314 We recognize the reported measurement bias of ice particle mass and concentration in
315 aircraft measurements. *Field et al.* [2006] notes that ice water content can be overestimated
316 by 20% - 30% by probes (which is not enough to account for the differences between the sim-
317 ulations and measurements presented here). The probes measure ice particles larger than 100
318 μm , and although shattering can cause ice concentrations to be positively biased, methods were
319 undertaken to compensate for any bias during data post-processing. It should be noted that the
320 ice crystals with diameters smaller than 100 μm are not expected to contribute significantly
321 to the ice mass mixing ratio, so shattering cannot account for observations being an order of
322 magnitude greater than the simulations in this study. Given this information, the measured ice
323 concentration should be lower than what is shown in Figure 4d, which makes the model bias
324 even higher.

325 Despite the differences in the magnitudes between the observed and simulated ice con-
326 centrations and masses, both schemes produce a mixed phase cloud with characteristics ob-
327 served during ISDAC: a liquid layer near cloud top and ice precipitation below. We assume

328 these are sufficient conditions to continue analysis regarding core properties of mixed-phase
329 clouds. We proceed with comparing the macrophysical properties of the cloud produced with
330 the subgrid-scale turbulence schemes in the next section.

331 **5 Control-Run Results with CLUBB and the 1.5-TKE Schemes**

332 The evolutions of the mixed-phase stratocumulus cloud during the 24-hour simulation
333 period for both the 1.5-TKE and CLUBB schemes are shown in Figure 5. As noted above,
334 CLUBB's predicted liquid water mass mixing ratio is smaller than the liquid water mass mix-
335 ing ratio predicted by the 1.5-TKE scheme. Further differences between the schemes can be
336 seen in the first few hours of the simulation as the model is spinning-up. While the 1.5-TKE
337 scheme has little-to-no liquid water in the first four hours (Figure 5a and Figure 5c), the CLUBB
338 scheme has both a liquid and ice profile. However as time progresses, the CLUBB cloud liq-
339 uid layer thins (Figure 5b), the cloud top decreases by 200 m, and eventually (if the simula-
340 tion is allowed to run longer than 24 hour) the cloud will dissipate to the point where the bound-
341 ary layer will not be capped by any liquid water or ice. Conversely, the 1.5-TKE scheme shows
342 positive cloud-top growth with increases in the liquid and ice water mass mixing ratios (Fig-
343 ure 5a and Figure 5e). The liquid layer depth increases in time (Figure 5a).

344 The mixed-phase cloud evolves into differing states (i.e., opaque cloud versus thin cloud)
345 depending on the scheme. The cloud with the 1.5-TKE scheme contains more liquid and is
346 more opaque than the cloud with CLUBB. This evolution has an effect on the downwelling
347 longwave surface flux. *Turner et al.* [2007] showed the longwave fluxes become insensitive
348 to increases in liquid water path for liquid water paths greater than about 40 g m^{-2} . Figure
349 6 shows the liquid water path of the mixed-phase cloud as a function of the computed down-
350 welling longwave surface flux. As the liquid water content with the 1.5-TKE simulation be-
351 comes established for liquid water paths $\geq 30 \text{ g m}^{-2}$, the downwelling longwave radiation
352 flux at the surface becomes constant at 260 W m^{-2} . However, the predicted liquid water path
353 when CLUBB is used is less than 15 g m^{-2} throughout the cloud's lifetime, peaking at the
354 beginning of the simulation.

355 The loss of liquid in the cloud produced by CLUBB without an increase in ice mass causes
356 the atmosphere to become more humid. Figure 7 shows this behavior in the profiles of the wa-
357 ter vapor mixing ratio, q_v , and the temperature, T , at 4, 10, 16, and 22 hours into the simu-
358 lation. The q_v profiles produced by CLUBB show a steep increase of water vapor between the

359 surface and 150 m which increases in time. We surmise the anomalously low value of $q_v \approx$
360 0 at the surface in the CLUBB simulation is a physical inconsistency that is intentionally in
361 the CLUBB scheme, and development efforts will be made to correct it. Recall surface-based
362 turbulent fluxes of heat and moisture were prescribed to be near-zero in these simulations, thus
363 little-to-no energy perturbations are available to lift the 1.5 g kg^{-1} of water vapor at 150 m
364 vertically to colder temperatures. Above 900 m, the cloud produced with CLUBB shows a larger
365 water vapor mixing ratio than the 1.5-TKE cloud, but low turbulent kinetic energies and ed-
366 dies (described further in Figure 8) will not entrain water vapor into the cloud top. Thus, the
367 water vapor is essentially not available to the cloud for condensation and particle growth. In
368 the simulation using the 1.5-TKE scheme, the surface value of q_v remains similar to the im-
369 posed initial condition value of 1.3 g kg^{-1} . The water vapor mixing ratio remains nearly con-
370 stant throughout the 24 hour simulation in the layer between 200 m to 600 m, which is be-
371 low the liquid layer. From 600 m to 800 m, q_v is depleted and is converted to liquid water.
372 Above 850 m, the water vapor concentration steadily decreases.

373 Moisture sources for the maintenance and stability of the mixed-phase cloud have been
374 explored by *Ovchinnikov et al.* [2011] and by *Solomon et al.* [2011]. *Ovchinnikov et al.* [2011]
375 shows that turbulent eddies from the cloud layer need to access the moisture at the surface if
376 the cloud is to persist. *Solomon et al.* [2011] found that the mixed-phase cloud is maintained
377 by a down-gradient transport of water vapor by turbulent fluxes from a specific humidity in-
378 version above the cloud top. *Qiu et al.* [2015] has confirmed an above-cloud moisture source
379 via three years of observations at the NSA site. CLUBB is not accessing either moisture source
380 above the cloud or below cloud base.

381 Stratocumulus clouds that are decoupled from the surface need a large-enough liquid wa-
382 ter path to drive in-cloud turbulence, which relates to the strength of the cloud-top tempera-
383 ture inversion. The lack of liquid in the CLUBB simulation (Figure 5b) affects the temper-
384 ature inversion at cloud top (Figure 7). The 1.5-TKE temperature inversion is 77% smaller than
385 the CLUBB inversion at 4 hours into the simulation (0.0318 K m^{-1} for 1.5-TKE compared
386 to 0.0414 K m^{-1} for CLUBB) due to CLUBB's more established liquid layer in the spin-up
387 period. However with CLUBB, at 22 hours into the simulation the cloud-top inversion decreases
388 nearly in half to 0.0235 K m^{-1} . Contrast this with 1.5-TKE scheme where the strength of the
389 temperature inversion increases to 0.0812 K m^{-1} . With CLUBB, the less-established liquid
390 layer results in reduced radiative cooling, which subsequently impacts the temperature inver-
391 sion, the cloud-top moisture jump, and the in-cloud dynamics. By the end of the simulation,

392 the liquid water path decreased from 6.5 g m^{-2} to 2 g m^{-2} compared to the 1.5-TKE scheme
393 which increased from 4 g m^{-2} to 54 g m^{-2} . Figure 7 shows that in the CLUBB simulation,
394 the moisture jump and the height of the temperature inversion decreases in time. This suggests
395 more water vapor is entrained to the area directly above the cloud top, creating a humid layer
396 above the temperature inversion. This is different from the 1.5-TKE situation, where the mois-
397 ture jump and temperature inversion strengthen in time.

398 The macroscopic differences just explained in the clouds' liquid water paths and opac-
399 ities produced by the two schemes is related to the amount of dissipative energy each subgrid
400 scheme calculates, which directly affects the energy of the boundary layer profile. We explain
401 a potential path to reducing the macrophysical differences in the clouds produced by the two
402 schemes in the next section. We will show that CLUBB's turbulence is more dissipative than
403 1.5-TKE turbulence and how to decrease the dissipation.

404 **6 Reducing CLUBB's Dissipative Energy**

405 The domain-averaged and time evolution of the resolved and subgrid-scale turbulent ki-
406 netic energies for the 1.5-TKE and CLUBB schemes are shown in Figure 8. CLUBB's resolved
407 and subgrid-scale turbulent kinetic energy is much smaller throughout the entire simulation
408 than the 1.5-TKE's kinetic energy with the exception of the first hour in the spin-up period.
409 At the surface, the CLUBB simulation's subgrid-scale turbulent kinetic energy is, at times, an
410 order of magnitude smaller than the 1.5-TKE simulation. At the end of the simulation, the do-
411 main averaged value for the resolved turbulent kinetic energy in the 1.5-TKE simulation is 0.15
412 $\text{m}^2 \text{ s}^{-2}$, whereas the CLUBB simulation is $0.03 \text{ m}^2 \text{ s}^{-2}$.

413 To see how subgrid-scale turbulent kinetic energy impacts the liquid water content, we
414 performed a sensitivity test by turning off the subgrid-scale turbulence parameterizations and
415 found that both the total kinetic energy and liquid water content decreased. For the CLUBB
416 scheme (Figures 8b and 8d), more kinetic energy is needed to maintain the liquid water path.
417 Reducing CLUBB's dissipative energy should increase the liquid water path of the cloud, which
418 can be achieved by two methods. The first is by increasing the length scale (Section 6.1), and
419 the second is by increasing the horizontal grid size (Section 6.2).

6.1 Increasing the Length Scale

The energy dissipated in the sub-grid scale needs to be reduced to increase the liquid water path. In CLUBB, energy dissipation, ϵ , is a function of the grid spacing (e.g. *Golaz et al.* [2002]). For example, energy dissipation for the vertical velocity variance, $\overline{w'^2}$, is computed from

$$\epsilon = \frac{C}{\tau} \overline{w'^2} - \nu \nabla^2 \overline{w'^2} \quad (2)$$

where the first term is a Newtonian damping term inversely proportional to a characteristic dissipation timescale, τ , and the second term is a background diffusion term used to damp small-scale noise and set to be much smaller than all other terms. In Equation 2, C and ν are constants set to control damping. The characteristic dissipation timescale, τ , is a ratio of the eddy length scale, L , and a characteristic velocity scale, given in Equation 2,

$$\tau = \frac{L}{\sqrt{\epsilon}}. \quad (3)$$

The length scale, L , is limited in CLUBB by the horizontal grid spacing, Δx and Δy , by $L = \alpha \min(\Delta x, \Delta y)$, where by default $\alpha = 0.25$ [*Larson et al.*, 2012]. To decrease dissipation in CLUBB, the length scale was increased to $L = 1.0 \min(\Delta x, \Delta y)$. This causes a larger value of τ , then a smaller Newtonian damping in Equation 3, and smaller energy dissipation, ϵ .

Increasing the limit on the length scale causes a 20-fold increase in liquid water path, a three-fold increase in ice water path, and a three-fold increase in resolved turbulent kinetic energy (Figure 9), which brings the macrophysical properties of the CLUBB simulation closer to the 1.5-TKE's and aircraft-measured properties. *Larson et al.* [2012] explains that in CLUBB, L represents the size of the large eddies. By choosing L to be a fraction of the grid box size, the host model will better-resolve the eddy motion. We can then infer that for the resolution chosen in this study ($\Delta x = \Delta y = 100$ m, $\Delta z = 20$ m), some eddies were not resolved. The sub-grid scale scheme needed to be more active at this resolution, and diagnosing a larger L improved the solution. We surmise, but have not tested, that a length scale between 0.25 and 1.0 might cause the liquid content to better-match the observed value.

6.2 Increasing Horizontal Grid Size

The horizontal grid size can also be increased to reduce the dissipative energy in CLUBB. We simulated the mixed-phase cloud using both the 1.5-TKE and CLUBB schemes over a range of increasing horizontal grid spacings from 50 m to 2500 m (Table 2). In all experiments, the model configuration and set-up is identical to what was described in Section 3 with the exception of the horizontal grid size. The liquid and ice water paths at the end of the simulation for both schemes are reported in Table 2. As expected, increasing the resolution when CLUBB is used causes the liquid water path to increase in the simulations when $\Delta x = 1000$ m and 2500 m (Figure 10). However, the cloud at these resolutions has too much turbulent kinetic energy and the liquid water path continues to increase, eventually exceeding the average aircraft value (16.2 g m^{-2}). The ice water path shows little-to-no sensitivity to resolution in the CLUBB scheme. We suspect this is due to the constraints on the ice number concentration (via Equation 2). The temperature inversion at $\Delta x = 2500$ m resolution with CLUBB is also stronger than at the control run resolution of 100 m (not shown). *Cheng et al.* [2010] has shown in simulations of warm stratocumulus clouds that liquid water path increases with resolution due to the energy (resolved and subgrid-scale) shifting to larger-scale with increased circulation.

The 1.5-TKE scheme produces a mixed-phase cloud at $\Delta x = 100$ and 1000 m grid resolutions and a mostly liquid cloud at 50 m resolution. At 2500 m resolution, the 1.5-TKE scheme has difficulty maintaining a steady-state mixed phase cloud with any ice water path. The overall sensitivity to resolution of mixed-phase clouds is best shown as the ratio of ice water path and liquid water path with increasing horizontal grid box size (Figure 11). Both schemes produce ratios that are at least a factor of three smaller than the aircraft measured values for all resolutions. CLUBB appears to converge with increasing Δx , implying a scale-awareness for $\Delta x \geq 1000$ m, whereas the 1.5-TKE scheme does not. Potential follow-on work would be understanding resolution convergence for each scheme while maintaining the macroscopic liquid and ice water paths of this mixed-phase cloud.

7 Properties of the Updraft and Downdraft Cores

Now that the macroscopic properties (i.e., liquid and ice water paths, temperature, and energy) of the mixed-phase cloud simulated by the two subgrid-scale turbulence schemes has been presented in the previous sections, we will show how these macroscopic properties im-

477 pact the core sizes, strength, and phase of the mixed phase cloud. This will answer our sec-
478 ond and third questions asked in Section 1.

479 First, the locations of the updraft and downdraft cores are identified with an algorithm
480 that marches through every point at every level at every time step. For a point to be classi-
481 fied as an updraft, two conditions are required: 1) the virtual potential temperature at an (x, y)
482 point has to be greater than the mean virtual potential temperature at that height, and 2) the
483 sum of the vertical velocity at that point and at the point height directly above it have to be
484 greater than zero. For an area to be classified as a downdraft, the opposite conditions are re-
485 quired. That is, 1) the virtual potential temperature at that (x, y) point has to be less than the
486 mean virtual potential temperature at that height, and 2) the sum of the vertical velocity at that
487 point and at the point directly above it have to be less than zero. If neither the updraft or down-
488 draft criteria are met, then the point is classified as having neutral vertical motion.

489 Cross-sectional snapshots of the locations identified as vertical velocity updrafts and down-
490 drafts are shown in Figures 12 and 13 for the cloud simulated with the 1.5 TKE and CLUBB
491 schemes, respectively. When the 1.5 TKE scheme is used, the updrafts and downdrafts appear
492 to organize themselves into larger areas of generally positive or generally negative vertical mo-
493 tion by 4 hours into the simulation for below cloud-base and throughout the domain at later
494 times in the simulation. (See, for example, Figures 12k, 12l, 12o, and 12p). This is meso- γ
495 scale organization of large areas of positive or negative vertical motion, and it has been ob-
496 served in other Arctic mixed-phase clouds [*Shupe et al.*, 2008]. Within the larger positive and
497 negative vertical motion areas are highly asymmetric and complex smaller cores. However,
498 the mixed-phase cloud produced with CLUBB is different: the updrafts and downdrafts remain
499 interspersed without larger organization and get weaker in time as the cloud dissipates. This
500 is consistent and to be expected given the lower turbulent kinetic energy and higher dissipa-
501 tion in the control-run CLUBB simulation. For reference, the domain-averaged updrafts and
502 downdrafts are shown for the 1.5-TKE and CLUBB simulations in Figure 14, again confirm-
503 ing the lower-energy CLUBB simulation produces weaker updrafts and downdrafts than the
504 1.5-TKE simulation.

505 Both simulations appear to produce the Rayleigh-Bénard convective cellular structures
506 as observed and documented in marine stratocumulus [*Feingold et al.*, 2010]. This means that
507 when the Rayleigh number exceeds its critical value ($Ra > Ra_c$), convection develops. The
508 Rayleigh number is given by $Ra = \alpha g \Delta T h^3 / (\nu \chi)$, where α is the thermal expansion coef-

509 efficient, g is the gravitational acceleration, h is the separation between two horizontal surfaces
510 with a temperature gradient, ν is the kinematic viscosity, and χ is the thermal diffusivity. For
511 atmospheric convection in stratiform clouds, ν and χ are replaced by eddy viscosity and eddy
512 diffusivity [Krishnamurti, 1975; Feingold *et al.*, 2010]. Assuming our domain is large enough
513 to contain a sample of organized convective cellular structures, this mixed-phase cloud has ap-
514 proximately a 10° C temperature gradient and a horizontal surface separation of approximately
515 1 km, giving $Ra \approx 10^6$, which exceeds $Ra_c \approx 10^3$. Thus, convective cellular structures are
516 supported in this cloud.

517 A closed-cellular convective structure is the preferred configuration for this cloud where
518 few, if no, cloud gaps are seen in the domain. The closed-cellular convective structure is best
519 seen in the three-dimensional snapshot of vertical velocity and precipitation in Figure 15 and
520 the Supporting Information Movie 1. The movie shows that the 1.5-TKE simulation produces
521 near-constant cloud cover where very few gaps in the cloud are seen in the domain. In mid-
522 latitude clouds, closed-cellular structures are driven by cooling at the cloud top with large ar-
523 eas of moderate updrafts and small areas with strong downdrafts [Helfand and Kalnay, 1983].
524 In autumn mixed-phase clouds, Shupe *et al.* [2008] reported a circulation pattern consisting
525 of strong, broad updrafts and weak, narrow downdrafts 5-8 km apart. The simulation produced
526 with the 1.5-TKE scheme has periodicity of ~ 5 km between updrafts and downdrafts of the
527 meso- γ scale organization (e.g. Figures 12 and 13), and the cloud produced with the CLUBB
528 scheme does not have this organization at all. In both simulations, however, there does not ap-
529 pear to be areas of narrow downdrafts as observed by Shupe *et al.* [2008]. We lack the obser-
530 vational datasets to claim if the organization seen in the 1.5-TKE scheme is realistic and if
531 it represents all springtime, decoupled stratocumulus mixed-phase cloud's convective organ-
532 ization.

533 This cloud's updraft and downdraft cores might be smaller than other closed-cell stra-
534 tocumulus due to the smaller precipitation rates and by corollary, strength of the downdrafts.
535 In simulations of autumn mixed-phase clouds, precipitation rates were nearly an order of mag-
536 nitude higher than the simulations here (~ 0.002 mm hr $^{-1}$ for 1.5-TKE mm hr $^{-1}$ and ~ 0.0006
537 for CLUBB) [Morrison *et al.*, 2008, 2011]. Additionally, precipitation rates in autumn mixed-
538 phase stratocumulus clouds appear to be more similar to midlatitude stratocumulus than this
539 springtime mixed-phase cloud [Feingold *et al.*, 2010; Wood, 2012].

540 The conceptual model of mixed-phase clouds in *Morrison et al.* [2012] suggests liquid
541 forms in updrafts, ice nucleates in the cloud layer, and then ice grows rapidly which encour-
542 ages sedimentation. To apply this conceptual model to our simulations, we once again assume
543 these simulations contain realistic aspects of the observed cloud in order to investigate the phase
544 partitioning within the updrafts and downdrafts. Individual core sizes are measured and iden-
545 tified with image processing software. Slices of the LES output at every level and timestep
546 are saved as portable network graphics (PNGs), and the cores are classified as “objects” by
547 the imaging processing software. Once identified as an “object”, the core size is computed from
548 the PNG at every level and timestep for both the 1.5-TKE and CLUBB schemes. Figure 16
549 shows the results of this computation, which is the domain-averaged mean updraft and down-
550 draft core sizes with the CLUBB and 1.5-TKE schemes. The ratio of the average size of the
551 cores is also presented in Figure 16. Both the 1.5-TKE and CLUBB schemes show that through-
552 out most of the simulation in the predominantly liquid portion of the cloud, the updraft cores
553 are bigger than the downdraft cores. This occurs between 600 m and 800 m in the cloud with
554 the 1.5-TKE scheme and roughly between 750 m and 600 m with the CLUBB scheme. Be-
555 low 600 m with both schemes, where the cloud is mostly ice, there are periodic times when
556 the downdraft cores are bigger than the updraft cores. Given what is seen in Figures 12, 13,
557 and 14, one can form an appended conceptual picture of this springtime mixed-phase cloud
558 where an “in-cloud” area might be thought-of distinct from the “below-cloud” area because
559 the average core-size ratio reverses in the column.

560 Figures 17 and 18 show a more detailed view of the phase of the updraft and downdraft
561 cores 10 hours into each simulation when the clouds are considered spun-up, but prior to sig-
562 nificant liquid water depletion when the CLUBB scheme is used. An important finding is that
563 both liquid and ice exist in both updraft and downdraft cores in both the CLUBB and 1.5-TKE
564 simulations. Liquid exists at the top of the cloud and then is depleted at lower levels (i.e., 100
565 m and 300 m). The rehumidification of the near-surface in the CLUBB simulation causes liq-
566 uid water to be present in the updraft core at 100 m, which does not exist in the simulation
567 when the 1.5-TKE scheme is used. Ice exists at all levels, is highest in concentration at 300
568 m and 600 m, and is depleted at the surface do to warmer temperatures. Ice is the dominant
569 phase in updaft and downdraft cores at all levels except at cloud top where liquid is dominant.
570 Once again appending to the *Morrison et al.* [2012] conceptual model of mixed-phase clouds,
571 we include ice to the top of the cloud base. Follow-on work would be to understand the size

572 of the ice in relation to the phase partitioning in other mixed phase stratocumulus clouds, such
573 as those that are coupled to the surface.

574 **8 Summary and Conclusions**

575 This study analyzes the macrophysical properties of an idealized springtime Arctic mixed-
576 phase stratocumulus cloud simulated with two different subgrid-scale turbulence schemes, 1.5-
577 TKE and CLUBB. We showed both schemes produced a stratocumulus mixed-phase cloud with
578 liquid at cloud top and ice precipitation towards the surface. These idealized simulations were
579 compared with in situ aircraft measurements to provide a basis for further analysis. This com-
580 parison revealed that the 1.5-TKE scheme produces an overly-liquid cloud and the CLUBB
581 scheme produces too little liquid water. Neither scheme was able to reproduce ice water mass
582 or number concentration within measurement variability. Both schemes underpredicted ice wa-
583 ter mass mixing ratio and overpredicted ice number concentration. This answered our first ques-
584 tion in Section 1, “What macroscopic differences arise in the cloud when different subgrid tur-
585 bulent parameterizations are used?”

586 We attribute differences in liquid water path and ice water path between the two schemes
587 to the amount of dissipative energy each subgrid scheme calculates. CLUBB is more dissi-
588 pative than 1.5-TKE, causing lower in-cloud resolved and subgrid-scale turbulent kinetic en-
589 ergy. To increase the amount of liquid water and turbulent kinetic energy in the mixed-phase
590 cloud with the CLUBB scheme, the turbulent length scale or the grid box size could be in-
591 creased. Increasing the grid box size (i.e., Δx and Δy), showed that CLUBB appears to be
592 more scale-aware than the 1.5-TKE scheme for $\Delta x, \Delta y > 1000$ m. This is consistent with
593 *Larson et al.* [2012], who tested CLUBB at kilometer-sized grid spacing and found improve-
594 ment in simulations of cumulus and boundary-layer clouds with increasing grid spacing. *Nishizawa*
595 *et al.* [2015] has had similar findings in that the grid aspect ratio influences the turbulent statis-
596 tics in the planetary boundary layer, and *Cheng et al.* [2010] found increasing the resolution in-
597 creases the liquid water path. As resolutions become higher in global models, there is a need
598 for understanding parameterization performance in many environments across many scales. Ex-
599 ploring the impact of changing grid geometries and resolution in simulations of Arctic stra-
600 tocumulus mixed-phase cloud is slated for future work.

601 We also asked in Section 1: “What are the properties (size, strength, and phase) of the
602 updraft and downdraft cores?” and “How do these properties compare with current knowledge
603 of other stratocumulus cloud cores?”

604 We found the 1.5-TKE scheme produces larger updraft cores and smaller downdraft cores
605 than the CLUBB scheme. In both schemes, the updraft cores are larger than the downdraft cores
606 in the liquid layer of the cloud. In the simulation with the CLUBB scheme, the downdraft cores
607 are bigger than the updraft cores in the ice precipitation portion of the cloud. However when
608 the 1.5-TKE scheme is used, downdraft cores are periodically bigger than updraft cores in the
609 ice precipitation portion of the cloud. From this relationship of core sizes throughout the col-
610 umn, a conceptual model is envisioned where two dominant areas of turbulent eddies exist:
611 one in the liquid portion of the cloud and the other in the ice precipitation portion of the cloud.
612 The cores in the 1.5-TKE scheme self-organize into a meso- γ circulation, which appears sim-
613 ilar to the configurations of closed-cell midlatitude and Arctic autumn mixed-phase stratocu-
614 mulus clouds. The cloud produced when the CLUBB scheme is used did not self-organize,
615 and the reason behind this could lie in the differences in the overall turbulent kinetic energy
616 in the cloud. These simulations imply this Arctic spring-time mixed-phase stratocumulus cloud’s
617 updraft and downdraft cores might generally have different sizes compared to closed-cell mid-
618 latitude and Arctic autumn mixed-phase stratocumulus clouds. Recall *Shupe et al.* [2008] re-
619 ported a circulation pattern consisting of strong, broad updrafts and weak, narrow downdrafts
620 5-8 km apart in autumn mixed-phase clouds. Midlatitude closed-cell stratocumulus are not (gen-
621 erally) mixed-phased, and it has been found that updraft cores are large but weak, whereas the
622 downdraft cores are small and strong [*Helfand and Kalnay*, 1983]. These differences are at-
623 tributed to lower precipitation rates in this springtime mixed-phase stratocumulus cloud com-
624 pared to other precipitating stratocumulus clouds.

625 The average strength of positive and negative vertical motion is similar within the scheme
626 used, and the 1.5-TKE scheme produces a cloud with stronger updrafts and downdrafts. We
627 analyzed the phase of the cores and found that liquid water mass exists in both updraft and
628 downdraft cores, but only in the top ~ 200 m of the cloud. Ice exists in both updraft and down-
629 draft cores from the surface to the cloud top in both schemes, maximizing at the base of the
630 liquid-layer in the updraft cores.

631 Limitations in our findings include the idealized nature of the simulations of this one spring-
632 time Arctic mixed-phase stratocumulus cloud and assumptions within the LES configuration

633 including the ice nucleation mechanism, aerosol size distribution and composition, and latent
634 heat release from ice formation in CLUBB. Additional sensitivity tests could emulate pertur-
635 bations of aerosols, temperature, and moisture, similar to the work of *Wang et al.* [2010] who
636 investigated drizzle formation in open cell, closed cell, and pockets of closed cells of stratocu-
637 mulus clouds in a larger domain. Follow-on work includes of resolution sensitivity and con-
638 vergence of cloud properties, similar to the methodology of *Cheng and Xu* [2008] and *Cheng*
639 *et al.* [2010]. With more observations and modeling of springtime mixed-phase stratocumu-
640 lus clouds, more knowledge can be obtained about these clouds and the relationship to their
641 environment.

642 **Acknowledgments**

643 The authors would like to thank the editor and two anonymous reviewers for their suggestions
644 which improved our manuscript. E. L. Roesler would also like to thank Mikhail Ovchinnikov,
645 Steven J. Ghan, Vince E. Larson, Leo Donner, and Alexei Korolev for their help and feedback
646 regarding SAM and ISDAC. We would like to thank Marat Khairoutdinov for providing the
647 System for Atmospheric Modeling (SAM). The Department of Energy's Global Change Ed-
648 ucation Program Graduate Research Environmental Fellowship and Sandia National Labora-
649 tories' Laboratory Directed Research and Development program funded this work. Data dis-
650 played in this paper will be curated for 5 years after publication and will be made available
651 upon request per AGU Publications Data Policy. Sandia National Laboratories is a multi-mission
652 laboratory managed and operated by Sandia Corporation, a wholly owned subsidiary of Lock-
653 heed Martin Corporation, for the U.S. Department of Energy's National Nuclear Security Ad-
654 ministration under contract DE-AC04-94AL85000. SAND201X-YYYY Z

655 **References**

- 656 Abdul-Razzak, H., and S. J. Ghan (2000), A parameterization of aerosol activation 2. mul-
657 tiple aerosol types, *Journal of Geophysical Research-Atmospheres*, *105*(D5), 6837–6844.
- 658 Avramov, A., and J. Y. Harrington (2010), Influence of parameterized ice habit on simu-
659 lated mixed-phase Arctic clouds, *Journal of Geophysical Research-Atmospheres*, *115*.
- 660 Avramov, A., A. S. Ackerman, A. M. Fridlind, B. van Dierenhoven, G. Botta, K. Aydin,
661 J. Verlinde, A. V. Korolev, J. W. Strapp, G. M. McFarquhar, R. Jackson, S. D. Brooks,
662 A. Glen, and M. Wolde (2011), Toward ice formation closure in Arctic mixed-phase
663 boundary layer clouds during ISDAC, *Journal of Geophysical Research-Atmospheres*,

664 116.

665 Barrie, L. A. (1986), Arctic air-pollution - an overview of current knowledge, *Atmospheric*
666 *Environment*, 20(4), 643–663.

667 Bogenschutz, P. A., A. Gettelman, H. Morrison, V. E. Larson, C. Craig, and D. P. Schanen
668 (2013), Higher-order turbulence closure and its impact on climate simulations in the
669 Community Atmosphere Model, *Journal of Climate*, 26(23), 9655–9676.

670 Cheng, A., K.-M. Xu, and B. Stevens (2010), Effects of resolution on the simulation of
671 boundary-layer clouds and the partition of kinetic energy to subgrid scales, *Journal of*
672 *Advances in Modeling Earth Systems*, 2(1), doi:10.3894/JAMES.2010.2.3, 3.

673 Cheng, A. N., and K. M. Xu (2008), Simulation of boundary-layer cumulus and stra-
674 tocumulus clouds using a cloud-resolving model with low- and third-order turbulence
675 closures, *Journal of the Meteorological Society of Japan*, 86a, 67–86.

676 Collins, W. D., P. J. Rasch, B. A. Boville, J. J. Hack, J. R. McCaa, D. L. Williamson,
677 B. P. Briegleb, C. M. Bitz, S.-J. Lin, and M. Zhang (2006), The formulation and atmo-
678 spheric simulation of the Community Atmosphere Model Version 3 (CAM3), *Journal of*
679 *Climate*, 19(11), 2144–2161.

680 Curry, J. A., W. B. Rossow, D. Randall, and J. L. Schramm (1996), Overview of Arctic
681 cloud and radiation characteristics, *Journal of Climate*, 9(8), 1731–1764.

682 de Boer, G., E. W. Eloranta, and M. D. Shupe (2009), Arctic mixed-phase stratiform
683 cloud properties from multiple years of surface-based measurements at two high-latitude
684 locations, *Journal of the Atmospheric Sciences*, 66(9), 2874–2887.

685 Deardorff, J. W. (1980), Stratocumulus-capped mixed layers derived from a 3-Dimensional
686 model, *Boundary-Layer Meteorology*, 18(4), 495–527.

687 Eicken, H. (2013), SEARCH: Study of Environmental Arctic Change,
688 <http://www.arcus.org/search/>.

689 European Centre for Medium-Range Weather Forecasts (2009), ERA-Interim, Project Re-
690 search Data Archive at the National Center for Atmospheric Research, Computational
691 and Information Systems Laboratory.

692 Fan, J. W., M. Ovtchinnikov, J. M. Comstock, S. A. McFarlane, and A. Khain (2009), Ice
693 formation in Arctic mixed-phase clouds: Insights from a 3-D cloud-resolving model
694 with size-resolved aerosol and cloud microphysics, *Journal of Geophysical Research-*
695 *Atmospheres*, 114.

- 696 Feingold, G., I. Koren, H. L. Wang, H. W. Xue, and W. A. Brewer (2010), Precipitation-
697 generated oscillations in open cellular cloud fields, *Nature*, 466(7308), 849–852.
- 698 Field, P. R., A. J. Heymsfield, and A. Bansemer (2006), Shattering and particle interar-
699 rival times measured by optical array probes in ice clouds, *Journal of Atmospheric and*
700 *Oceanic Technology*, 23(10), 1357–1371.
- 701 Francis, J. A., and S. J. Vavrus (2012), Evidence linking Arctic amplification to
702 extreme weather in mid-latitudes, *Geophysical Research Letters*, 39(6), doi:
703 10.1029/2012GL051000.
- 704 Ghan, S. J. (2010), Personal communication.
- 705 Ghan, S. J., B. Schmid, J. Hubbe, C. Flynn, A. Laskin, A. Zelenyuk, D. Czizco, C. Long,
706 G. McFarquhar, J. Verlinde, J. Harrington, W. Strapp, P. Liu, A. Korolev, A. McDonald,
707 M. Wolde, A. Fridlind, T. Garrett, G. Mace, G. Kok, S. Brooks, D. Collins, D. Lubin,
708 P. Lawson, M. Dubey, C. Mazzoleni, M. Shupe, S. Xie, D. Turner, Q. Min, E. Mlawer,
709 and D. Mitchell (2007), Science overview document Indirect and Semi-Direct Aerosol
710 Campaign (ISDAC) April 2008.
- 711 Golaz, J. C., V. E. Larson, and W. R. Cotton (2002), A PDF-based model for boundary
712 layer clouds. Part I: Method and model description, *Journal of the Atmospheric Sciences*,
713 59(24), 3540–3551.
- 714 Helfand, H. M., and E. Kalnay (1983), A model to determine open or closed cellular
715 convection, *Journal of the Atmospheric Sciences*, 40(3), 631–650.
- 716 Intrieri, J. M., C. W. Fairall, M. D. Shupe, P. O. G. Persson, E. L. Andreas, P. S. Guest,
717 and R. E. Moritz (2002), An annual cycle of Arctic surface cloud forcing at SHEBA,
718 *Journal of Geophysical Research-Oceans*, 107(C10).
- 719 Khairoutdinov, M. F., and D. A. Randall (2003), Cloud resolving modeling of the ARM
720 summer 1997 IOP: Model formulation, results, uncertainties, and sensitivities, *Journal*
721 *of the Atmospheric Sciences*, 60(4), 607–625.
- 722 Klein, S. A., R. B. McCoy, H. Morrison, A. S. Ackerman, A. Avramov, G. d. Boer,
723 M. Chen, J. N. S. Cole, A. D. Del Genio, M. Falk, M. J. Foster, A. Fridlind, J.-C.
724 Golaz, T. Hashino, J. Y. Harrington, C. Hoose, M. F. Khairoutdinov, V. E. Larson,
725 X. Liu, Y. Luo, G. M. McFarquhar, S. Menon, R. A. J. Neggers, S. Park, M. R. Poellot,
726 J. M. Schmidt, I. Sednev, B. J. Shipway, M. D. Shupe, D. A. Spangenberg, Y. C. Sud,
727 D. D. Turner, D. E. Veron, K. v. Salzen, G. K. Walker, Z. Wang, A. B. Wolf, S. Xie,
728 K.-M. Xu, F. Yang, and G. Zhang (2009), Intercomparison of model simulations of

- 729 mixed-phase clouds observed during the ARM Mixed-Phase Arctic Cloud Experiment
730 I: Single-layer cloud, *Quarterly Journal of the Royal Meteorological Society*, 135(641),
731 979–1002.
- 732 Krishnamurti, R. (1975), On cellular cloud patterns. Part 1: Mathematical model, *Journal*
733 *of the Atmospheric Sciences*, 32(7), 1353–1363.
- 734 Larson, V. E., J.-C. Golaz, and W. R. Cotton (2002), Small-scale and mesoscale vari-
735 ability in cloudy boundary layers: Joint probability density functions, *Journal of the*
736 *Atmospheric Sciences*, 59(24), 3519–3539.
- 737 Larson, V. E., D. P. Schanen, M. H. Wang, M. Ovchinnikov, and S. Ghan (2012), PDF
738 parameterization of boundary layer clouds in models with horizontal grid spacings from
739 2 to 16 km, *Monthly Weather Review*, 140(1), 285–306.
- 740 McFarquhar, G. M., G. Zhang, M. R. Poellot, G. L. Kok, R. McCoy, T. Tooman,
741 A. Fridlind, and A. J. Heymsfield (2007), Ice properties of single-layer stratocumu-
742 lus during the Mixed-Phase Arctic Cloud Experiment: 1. Observations, *Journal of*
743 *Geophysical Research-Atmospheres*, 112(D24).
- 744 McFarquhar, G. M., S. Ghan, J. Verlinde, A. Korolev, J. W. Strapp, B. Schmid, J. M.
745 Tomlinson, M. Wolde, S. D. Brooks, D. Cziczo, M. K. Dubey, J. W. Fan, C. Flynn,
746 I. Gultepe, J. Hubbe, M. K. Gilles, A. Laskin, P. Lawson, W. R. Leitch, P. Liu,
747 X. H. Liu, D. Lubin, C. Mazzoleni, A. M. Macdonald, R. C. Moffet, H. Morrison,
748 M. Ovchinnikov, M. D. Shupe, D. D. Turner, S. C. Xie, A. Zelenyuk, K. Bae, M. Freer,
749 and A. Glen (2011), Indirect and Semi-Direct Aerosol Campaign: The impact of Arctic
750 aerosols on clouds, *Bulletin of the American Meteorological Society*, 92(2).
- 751 Morrison, H., J. A. Curry, and V. I. Khvorostyanov (2005), A new double-moment micro-
752 physics parameterization for application in cloud and climate models. Part I: Descrip-
753 tion, *Journal of the Atmospheric Sciences*, 62(6), 1665–1677.
- 754 Morrison, H., J. O. Pinto, J. A. Curry, and G. M. McFarquhar (2008), Sensitivity of
755 modeled Arctic mixed-phase stratocumulus to cloud condensation and ice nuclei over
756 regionally varying surface conditions, *Journal of Geophysical Research-Atmospheres*,
757 113(D5).
- 758 Morrison, H., P. Zuidema, A. S. Ackerman, A. Avramov, G. de Boer, J. W. Fan, A. M.
759 Fridlind, T. Hashino, J. Y. Harrington, Y. L. Luo, M. Ovchinnikov, and B. Shipway
760 (2011), Intercomparison of cloud model simulations of Arctic mixed-phase boundary
761 layer clouds observed during SHEBA/FIRE-ACE, *Journal of Advances in Modeling*

- 762 *Earth Systems*, 3.
- 763 Morrison, H., G. de Boer, G. Feingold, J. Harrington, M. D. Shupe, and K. Sulia (2012),
764 Resilience of persistent Arctic mixed-phase clouds, *Nature Geoscience*, 5(1), 11–17.
- 765 Nishizawa, S., H. Yashiro, Y. Sato, Y. Miyamoto, and H. Tomita (2015), Influence of grid
766 aspect ratio on planetary boundary layer turbulence in large-eddy simulations, *Geosci.*
767 *Model Dev.*, 8(10), 3393–3419, doi:10.5194/gmd-8-3393-2015.
- 768 Orlandi, I. (1975), Rational subdivision of scales for atmospheric processes, *Bulletin of*
769 *the American Meteorological Society*, 56(5), 527–530.
- 770 Ovchinnikov, M., A. Korolev, and J. W. Fan (2011), Effects of ice number concentra-
771 tion on dynamics of a shallow mixed-phase stratiform cloud, *Journal of Geophysical*
772 *Research-Atmospheres*, 116.
- 773 Ovchinnikov, M., A. S. Ackerman, A. Avramov, A. Cheng, J. Fan, A. M. Fridlind,
774 S. Ghan, J. Harrington, C. Hoose, A. Korolev, G. M. McFarquhar, H. Morrison,
775 M. Paukert, J. Savre, B. J. Shipway, M. D. Shupe, A. Solomon, and K. Sulia (2014),
776 Intercomparison of large-eddy simulations of Arctic mixed-phase clouds: Importance of
777 ice size distribution assumptions, *Journal of Advances in Modeling Earth Systems*.
- 778 Qiu, S. Y., X. Q. Dong, B. Xi, and J. L. F. Li (2015), Characterizing Arctic mixed-phase
779 cloud structure and its relationship with humidity and temperature inversion using ARM
780 NSA observations, *Journal of Geophysical Research-Atmospheres*, 120(15), 7737–7746,
781 doi:10.1002/2014jd023022.
- 782 Roesler, E. L., and J. E. Penner (2010), Can global models ignore the chemical composi-
783 tion of aerosols?, *Geophysical Research Letters*, 37.
- 784 Shupe, M. D., T. Uttal, and S. Y. Matrosov (2005a), Arctic cloud microphysics retrievals
785 from surface-based remote sensors at SHEBA, *Journal of Applied Meteorology*, 44(10),
786 1544–1562.
- 787 Shupe, M. D., T. Uttal, and S. Y. Matrosov (2005b), Arctic cloud microphysics retrievals
788 from surface-based remote sensors at SHEBA, *Journal of Applied Meteorology*, 44(10),
789 1544–1562.
- 790 Shupe, M. D., S. Y. Matrosov, and T. Uttal (2006), Arctic mixed-phase cloud properties
791 derived from surface-based sensors at SHEBA, *Journal of the Atmospheric Sciences*,
792 63(2), 697–711.
- 793 Shupe, M. D., P. Kollias, P. O. G. Persson, and G. M. McFarquhar (2008), Vertical mo-
794 tions in Arctic mixed-phase stratiform clouds, *Journal of the Atmospheric Sciences*,

795 65(4), 1304–1322.

796 Shupe, M. D., P. O. G. Persson, I. M. Brooks, M. Tjernström, J. Sedlar, T. Mauritsen,
797 S. Sjogren, and C. Leck (2013), Cloud and boundary layer interactions over the Arctic
798 sea ice in late summer, *Atmos. Chem. Phys.*, *13*(18), 9379–9399.

799 Solomon, A., M. D. Shupe, P. O. G. Persson, and H. Morrison (2011), Moisture and dy-
800 namical interactions maintaining decoupled Arctic mixed-phase stratocumulus in the
801 presence of a humidity inversion, *Atmospheric Chemistry and Physics*, *11*(19), 10,127–
802 10,148.

803 Storer, R. L., B. M. Griffin, J. Höft, J. K. Weber, E. Raut, V. E. Larson, M. Wang, and
804 P. J. Rasch (2015), Parameterizing deep convection using the assumed probability den-
805 sity function method, *Geoscientific Model Development*, *8*(1), 1–19, doi:10.5194/gmd-8-
806 1-2015.

807 Stroeve, J. C., V. Kattsov, A. Barrett, M. Serreze, T. Pavlova, M. Holland, and W. N.
808 Meier (2012), Trends in Arctic sea ice extent from CMIP5, CMIP3 and observations,
809 *Geophysical Research Letters*, *39*.

810 Sulia, K. J., H. Morrison, and J. Y. Harrington (2014), Dynamical and microphysical
811 evolution during mixed-phase cloud glaciation simulated using the bulk adaptive habit
812 prediction model, *Journal of the Atmospheric Sciences*, *71*(11), 4158–4180.

813 Turner, D. D., A. M. Vogelmann, K. Johnson, M. Miller, R. T. Austin, J. C. Barnard,
814 C. Flynn, C. Long, S. A. McFarlane, K. Cady-Pereira, S. A. Clough, J. C. Chiu,
815 M. M. Khaiyer, J. Liljegren, B. Lin, P. Minnis, A. Marshak, S. Y. Matrosov, Q. Min,
816 W. O'Hirok, Z. Wang, and W. Wiscombe (2007), Thin liquid water clouds: Their im-
817 portance and our challenge, *Bulletin of the American Meteorological Society*, *88*(2),
818 177–190.

819 Wang, H., G. Feingold, R. Wood, and J. Kazil (2010), Modelling microphysical and
820 meteorological controls on precipitation and cloud cellular structures in southeast
821 pacific stratocumulus, *Atmospheric Chemistry and Physics*, *10*(13), 6347–6362, doi:
822 10.5194/acp-10-6347-2010.

823 Wood, R. (2012), Stratocumulus clouds, *Monthly Weather Review*, *140*(8), 2373–2423,
824 doi:10.1175/MWR-D-11-00121.1.

825 Xie, S. C., S. A. Klein, M. H. Zhang, J. J. Yio, R. T. Cederwall, and R. McCoy (2006),
826 Developing large-scale forcing data for single-column and cloud-resolving models
827 from the Mixed-Phase Arctic Cloud Experiment, *Journal of Geophysical Research-*

840 **Table 1.** Vertical prognostic quantities in the 1.5-TKE scheme based on *Deardorff* [1980] and the CLUBB
 841 scheme from *Golaz et al.* [2002] where w is the vertical velocity, θ_l is the liquid water potential temperature,
 842 and q_t is the total water specific humidity.

Scheme	$\overline{w'\theta'_l}$	$\overline{w'q'_t}$	$\overline{q'_t\theta'_l}$	$\overline{w'^2}$	$\overline{\theta_l'^2}$	$\overline{q_t'^2}$	$\overline{w'^3}$
1.5-TKE	×	×		×			
CLUBB	×	×	×	×	×	×	×

843 **Table 2.** Horizontal grid box sizes and domain sizes of resolution sensitivity tests with the liquid water
 844 path and ice water path at the end of the simulation for each resolution test.

Horizontal Grid Box Size $\Delta x \times \Delta y \times \Delta z$	Domain Size on an Edge (km)	Liquid Water Path (g m^{-2})		Ice Water Path (g m^{-2})	
		at 24 hours		at 24 hours	
		1.5-TKE	CLUBB	1.5-TKE	CLUBB
50 m \times 50 m \times 20 m	6	72.5	9.60	0.08	0.12
100 m \times 100 m \times 20 m	12	56.7	2.67	2.33	0.74
1000 m \times 1000 m \times 20 m	120	62.4	47.8	2.55	1.65
2500 m \times 2500 m \times 20 m	300	0.59	47.7	0.006	1.18

845 **Figure 1.** The fractional cloud cover at approximately 865 hPa over the Arctic on 26 April 2008 at 06:00
 846 GMT taken from the ERA-40 Interim reanalysis. The gold star indicates the location of Barrow, Alaska.

828 *Atmospheres*, 111(D19).

829 Zelenyuk, A., D. Imre, M. Earle, R. Easter, A. Korolev, R. Leitch, P. Liu, A. M. Mac-
 830 donald, M. Ovchinnikov, and W. Strapp (2010), In situ characterization of cloud con-
 831 densation nuclei, interstitial, and background particles using the single particle mass
 832 spectrometer, SPLAT II, *Analytical Chemistry*, 82(19), 7943–7951.

833 Zhang, M. H., and J. L. Lin (1997), Constrained variational analysis of sounding data
 834 based on column-integrated budgets of mass, heat, moisture, and momentum: Approach
 835 and application to ARM measurements, *Journal of the Atmospheric Sciences*, 54(11),
 836 1503–1524.

837 Zhang, M. H., J. L. Lin, R. T. Cederwall, J. J. Yio, and S. C. Xie (2001), Objective
 838 analysis of ARM IOP data: Method and sensitivity, *Monthly Weather Review*, 129(2),
 839 295–311.

847 **Figure 2.** Idealized vertical profiles used for model initialization and large-scale forcing. From left to
 848 right, a) temperature (T), b) water vapor mixing ratio (q_v), c) zonal wind (u), d) meridional wind (v), and e)
 849 large-scale vertical wind (w).

850 **Figure 3.** Snapshots of the cross section of the vertical velocity in the 1.5-TKE simulation at a) 2 hours and
 851 b) 4 hours. The cross section is taken in the middle of the domain at $y = 6000$ m.

852 **Figure 4.** Comparison of the profiles of the average of the aircraft measurements (dots) with the average of
 853 the simulations using the 1.5-TKE scheme (solid line) and CLUBB (dashed line) for the a) liquid water mass
 854 mixing ratio, b) liquid number concentration, c) ice water mass mixing ratio, and d) ice number concentration.
 855 The aircraft measurements were binned into the model's vertical grid levels and plotted here at each mid-point
 856 of the model's vertical grid levels. The horizontal lines on the dots are the standard deviation of the mean of
 857 the measurements.

858 **Figure 5.** Evolution of the domain-averaged cloud profiles by height of a) - b) liquid water mass mixing
 859 ratio, c) - d) liquid number concentration, e) - f) ice water mass mixing ratio, and g) - h) ice number concen-
 860 tration for the 1.5-TKE scheme (left) and the CLUBB (right) during the 24-hour simulation period.

861 **Figure 6.** Downwelling longwave radiation flux at the surface as a function of liquid water path for the 1.5-
 862 TKE (dots) and CLUBB (plus-marks) mixed-phase clouds. Each data point represents the domain-averaged
 863 value every 600 seconds in time.

864 **Figure 7.** Profiles of the domain-averaged water vapor mixing ratio, q_v (dashed), and temperature, T
 865 (solid), from the 1.5-TKE (in black) and CLUBB (in red) schemes. The profiles are at a) 4, b) 10, c) 16, and
 866 d) 22 hours into the simulation.

867 **Figure 8.** The domain-averaged time evolution by height of the resolved (a) and b)) and subgrid-scale (c)
 868 and d)) turbulent kinetic energy profiles in time for the 1.5-TKE (a) and c)) and CLUBB (b) and d)) schemes.

869 **Figure 9.** Domain-averaged a) liquid water path, b) ice water path, and c) resolved turbulent kinetic energy
 870 in time for the mixed-phase clouds produced by using the 1.5-TKE scheme (black solid line), CLUBB with
 871 the default length scale limitation (red large dash line), and CLUBB with a four-fold increase in the length
 872 scale limitation (red small dash line). The average of the aircraft measurements for liquid and ice water paths
 873 is shown as a solid blue line in a) and b) in time for comparison.

874 **Figure 10.** Domain-averaged liquid water path (a and b)) and ice water path (c and d)) in time with var-
 875 ious horizontal grid box sizes for the 1.5-TKE (left) and CLUBB (right) schemes. The average liquid water
 876 path and ice water path from the aircraft measurements is shown as a solid line (Meas) for comparison in each
 877 of the plots.

878 **Figure 11.** Changes to the ratio of ice water path to liquid water path as horizontal grid box size is in-
 879 creased when the 1.5-TKE (asterisk) and CLUBB (dots) schemes are used. The aircraft value is shown for
 880 comparison as a solid line (Meas).

881 **Figure 12.** Snapshots of the vertical velocity (m s^{-1}) in the updraft (red) and downdraft (blue) cores taken
 882 at 4, 10, 16, and 22 hours into the simulation at 100, 300, 600, and 800 m above the surface while using the
 883 1.5-TKE scheme.

884 **Figure 13.** Snapshots of the vertical velocity (m s^{-1}) in the updraft (red) and downdraft (blue) cores taken
 885 at 4, 10, 16, and 22 hours into the simulation at 100, 300, 600, and 800 m above the surface while using the
 886 CLUBB scheme.

887 **Figure 14.** Profiles of the domain-averaged upward and downward vertical velocity, with the 1.5-TKE (in
 888 black) and CLUBB (in red) schemes. The profiles are at a) 4, b) 10, c) 16, and d) 22 hours into the simulation.

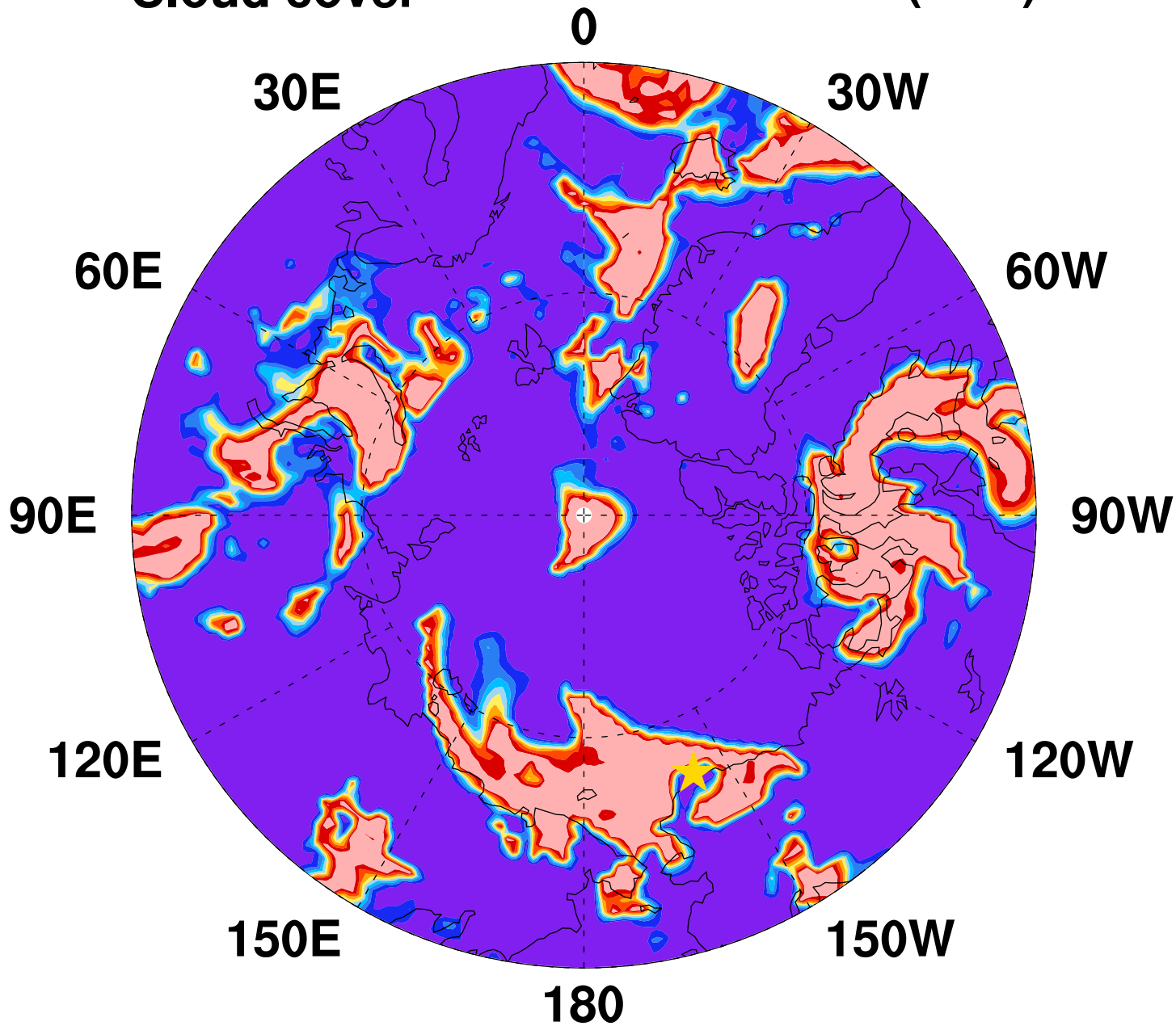
889 **Figure 15.** Total condensate (precipitating rain and snow and nonprecipitating water and ice) and the verti-
 890 cal velocity at 12 hours into the simulation for the 1.5 TKE scheme (left) and the CLUBB scheme (right). The
 891 total condensate is shown in the rainbow colorbar, and the vertical velocity is shown with the blue-to-red color
 892 bar.

893 **Figure 16.** Ratio of the average updraft and downdraft core size for the entire domain in height as a func-
 894 tion of time for the a) 1.5 TKE scheme and b) CLUBB scheme. The domain-averaged downdraft and updraft
 895 core sizes are shown for the 1.5 TKE scheme (c) and d), respectively), and the CLUBB scheme (e) and f),
 896 respectively). Please note the values of the colorbars are different in c), d), e), and f).

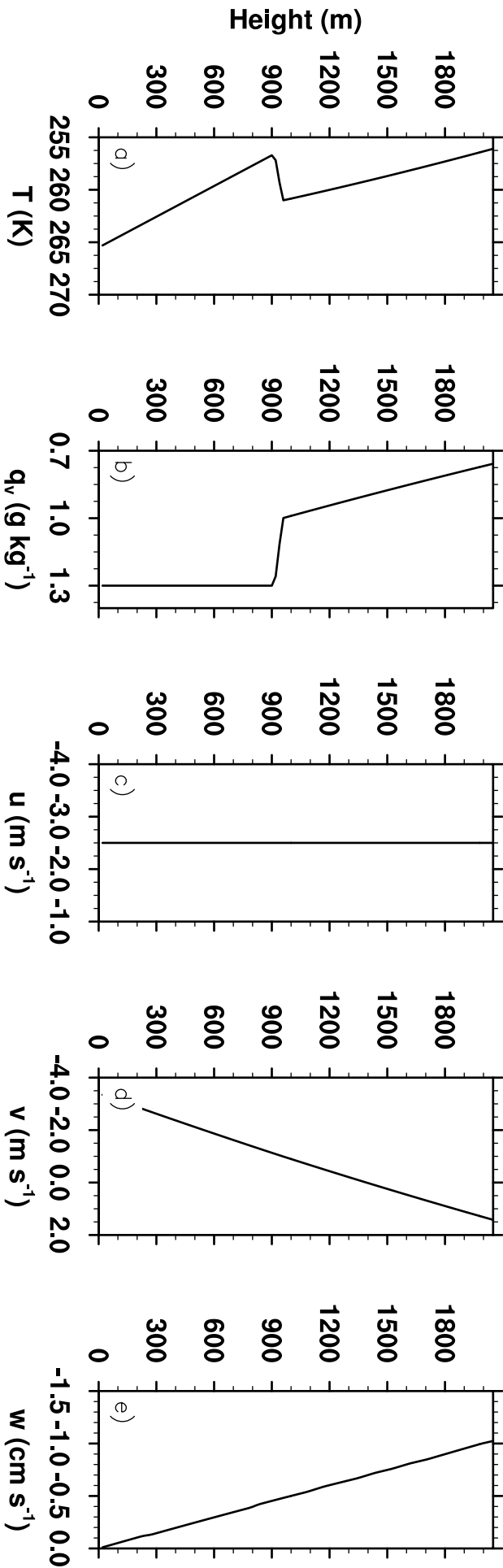
897 **Figure 17.** The liquid and ice water contents (g kg^{-1}) in the updraft and downdraft cores at 100, 300, 600,
898 and 800 m above the surface, 10 hours into the simulation for when the 1.5-TKE scheme was used. The mean
899 value of each contour plot is given at the top of each contour plot.

900 **Figure 18.** The liquid and ice water contents (g kg^{-1}) in the updraft and downdraft cores at 100, 300, 600,
901 and 800 m above the surface, 10 hours into the simulation for when the CLUBB scheme was used. The mean
902 value of each contour plot is given at the top of each contour plot.

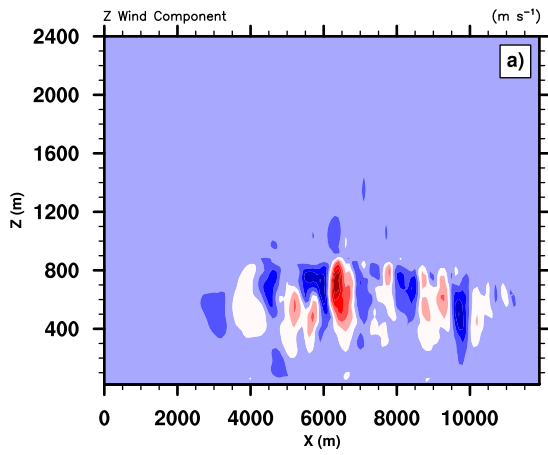
Cloud cover (0 - 1)



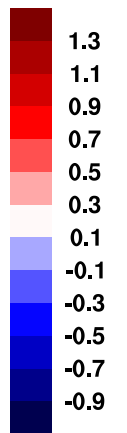
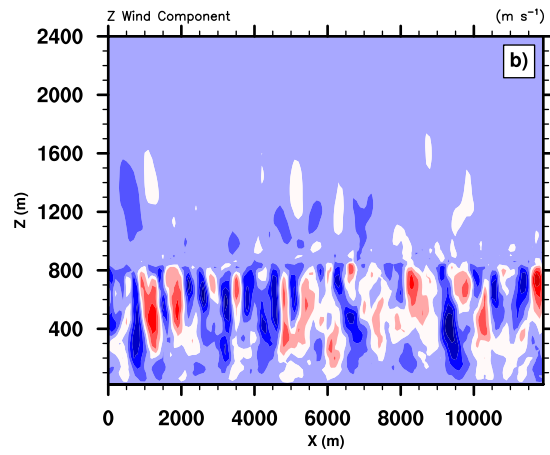
0.1 0.2 0.3 0.4 0.5 0.6 0.7 0.8 0.9

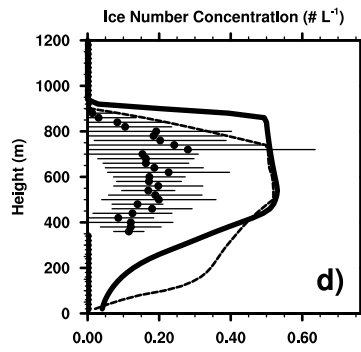
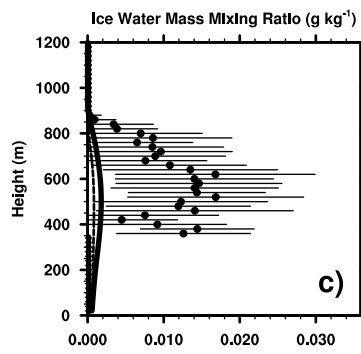
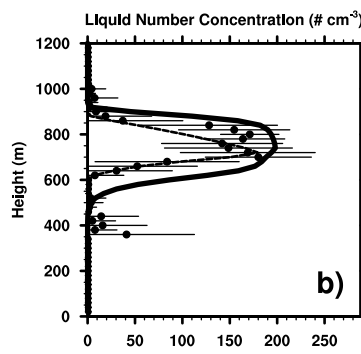
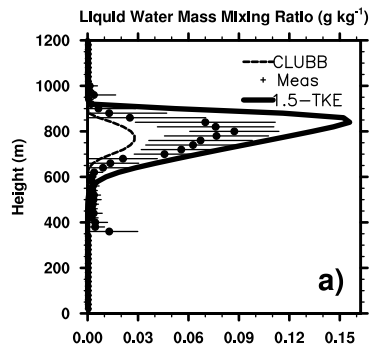


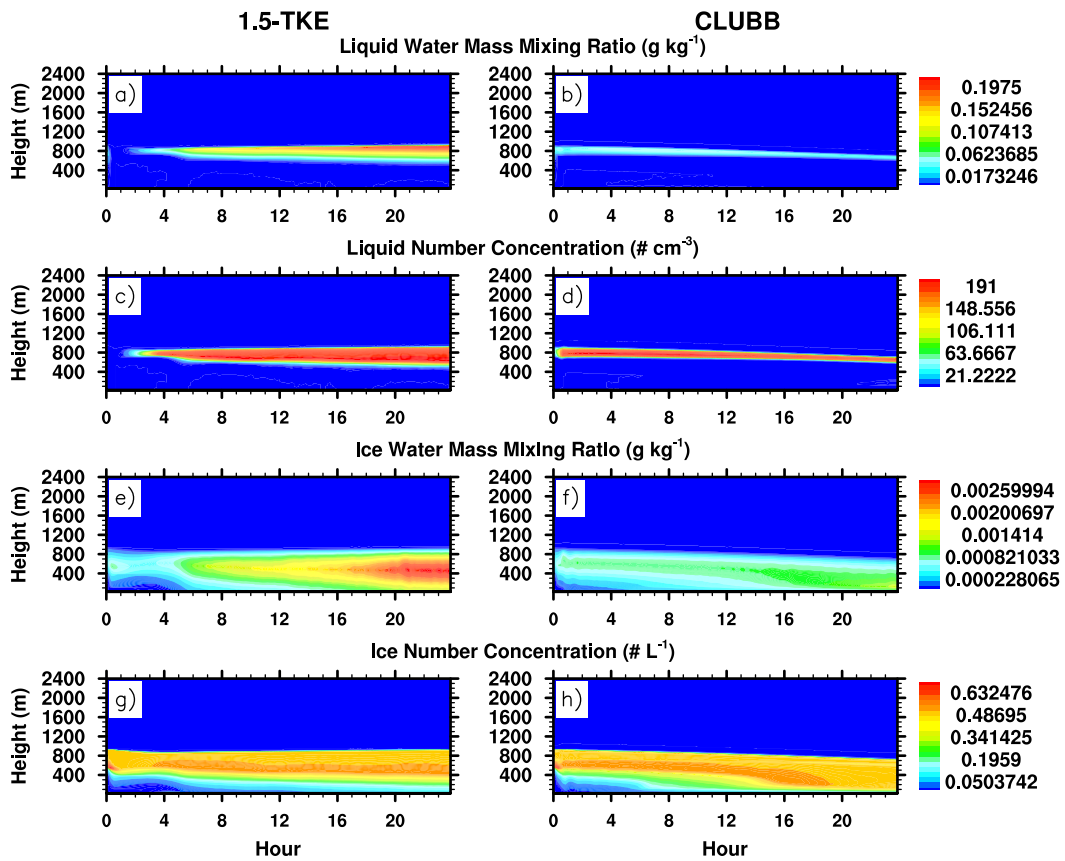
Time = 2 hours



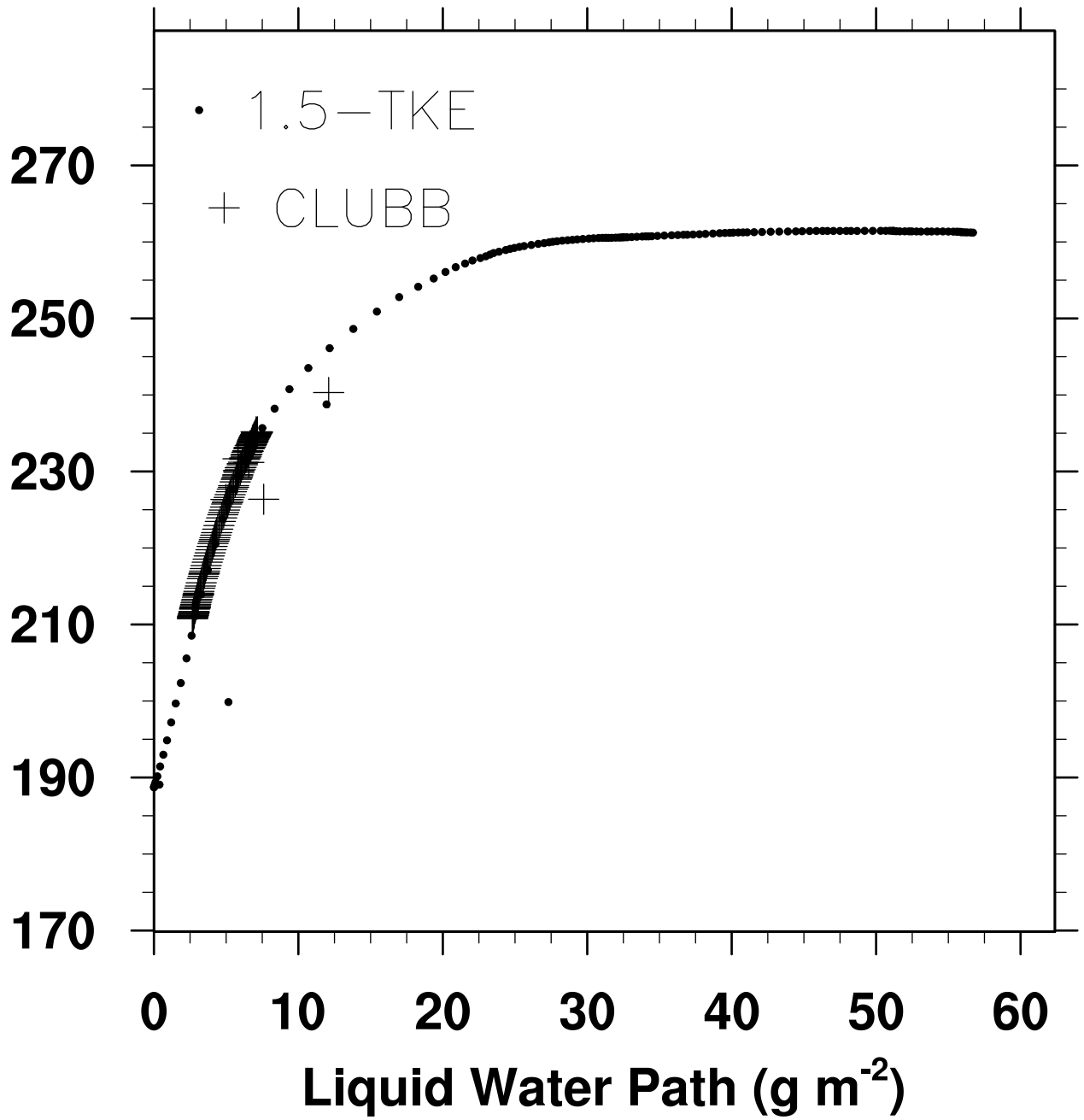
Time = 4 hours

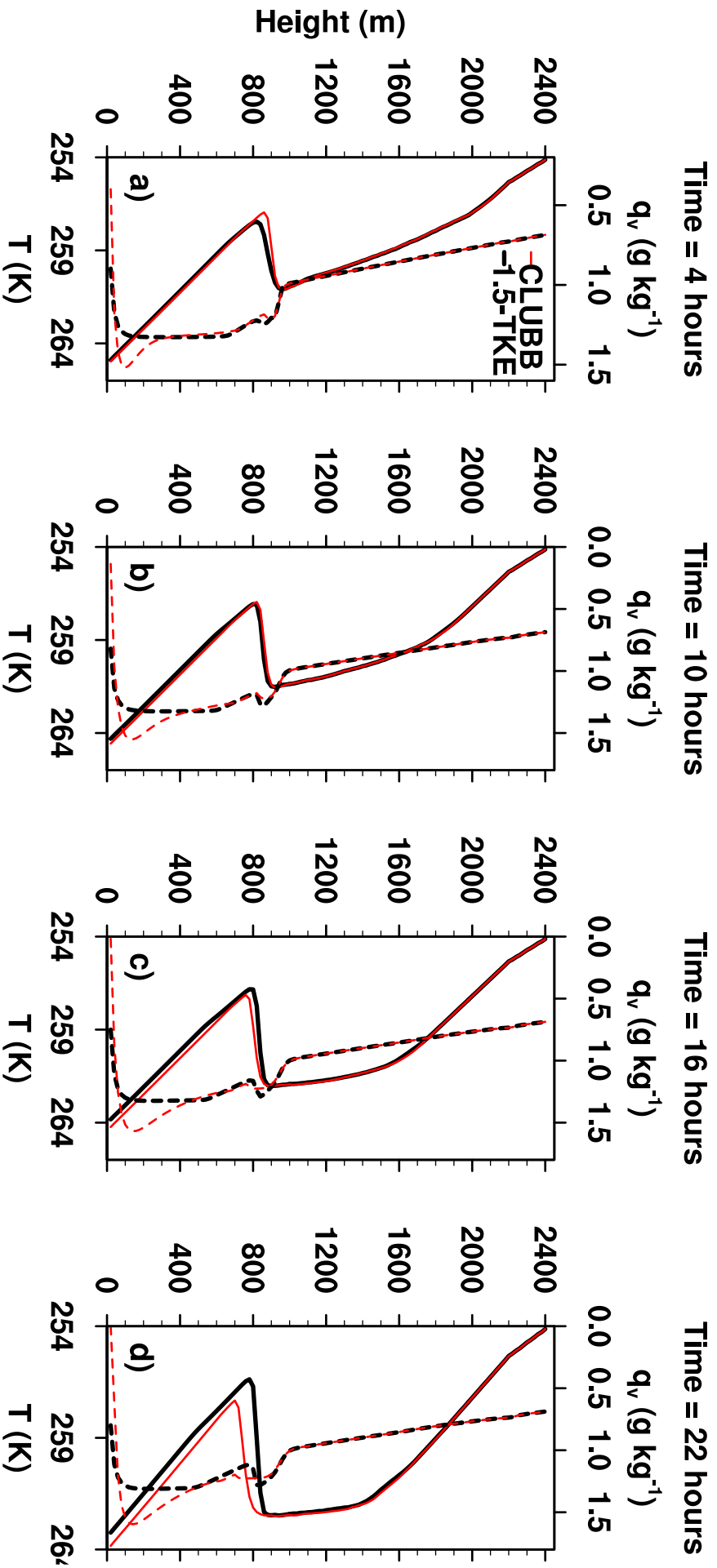


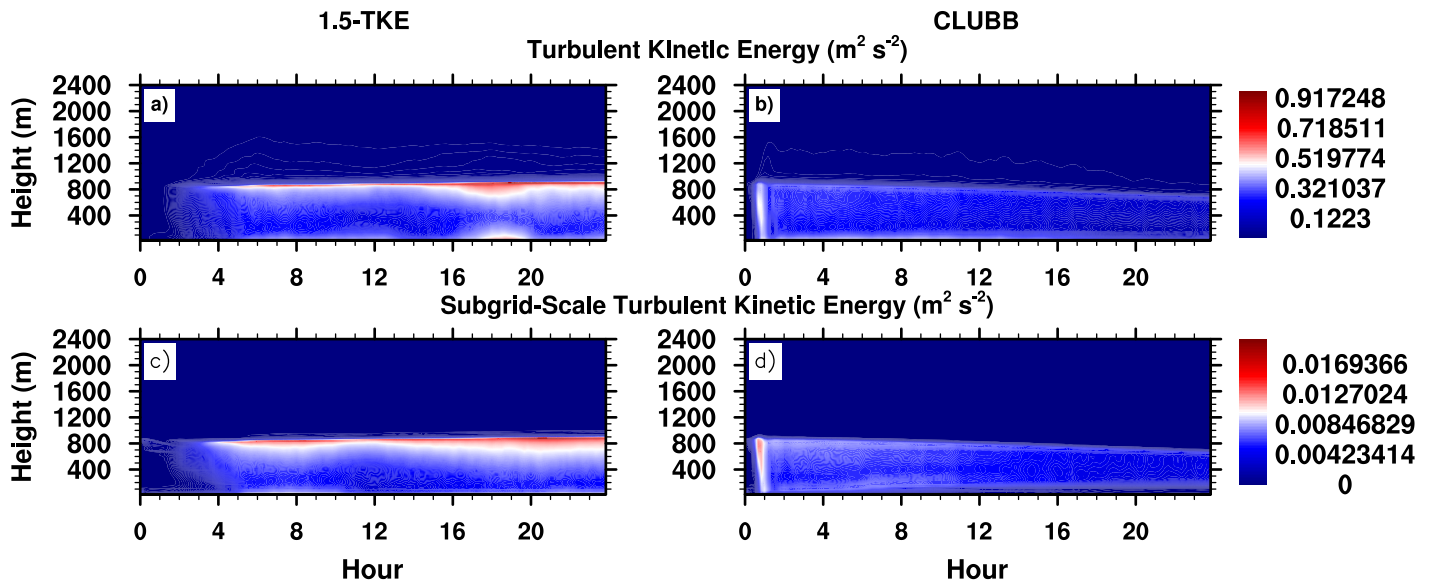


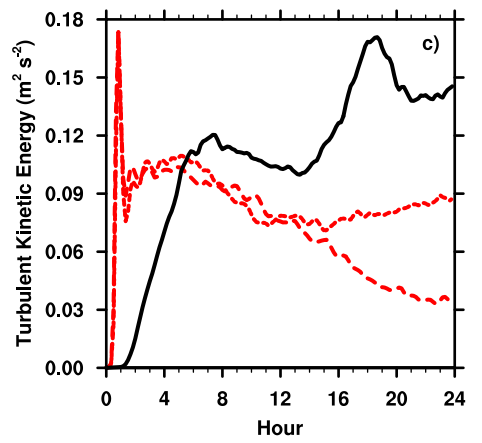
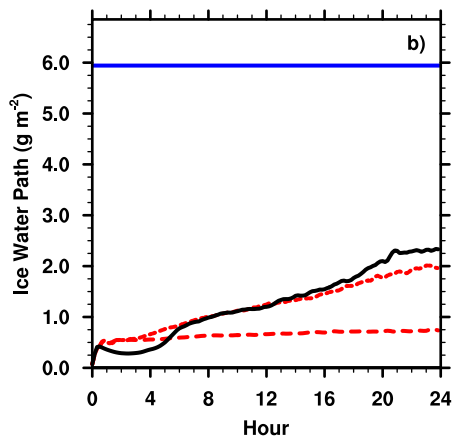
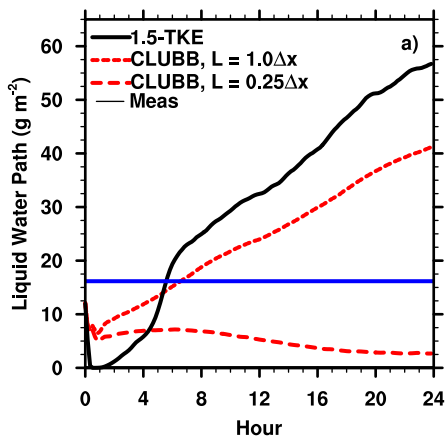


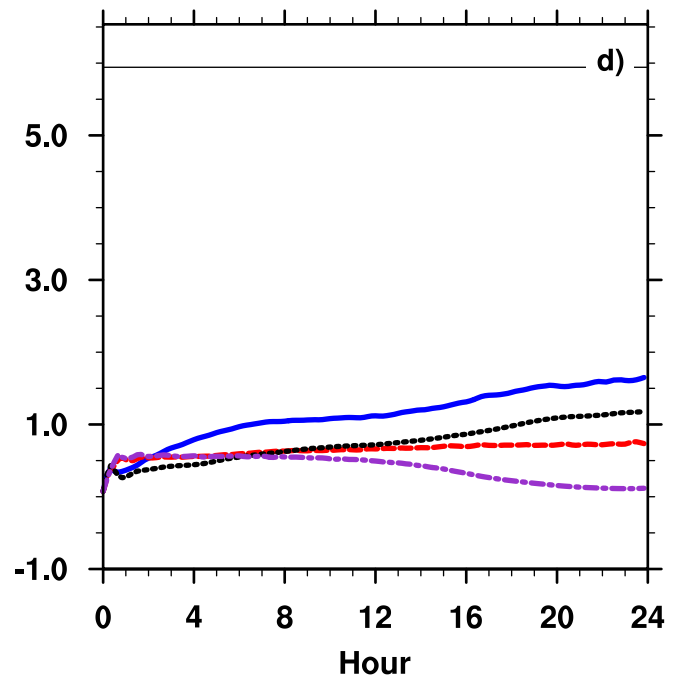
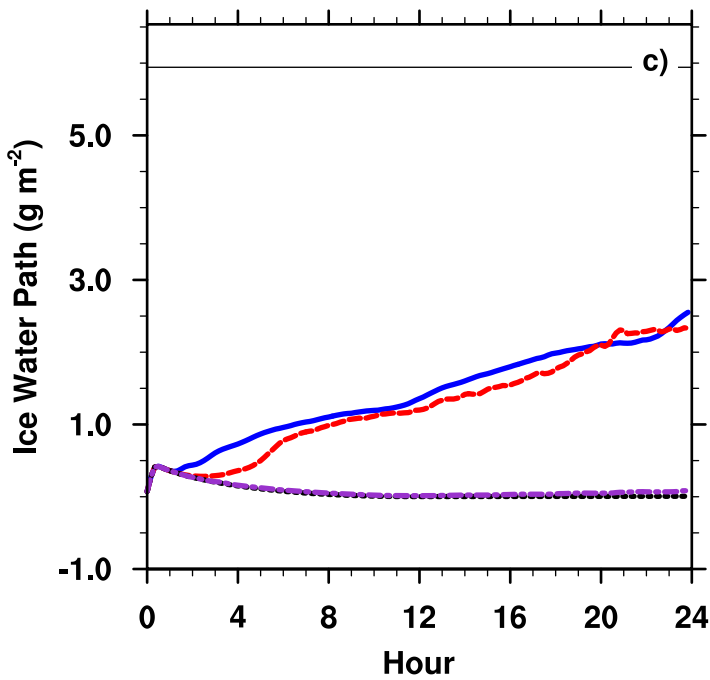
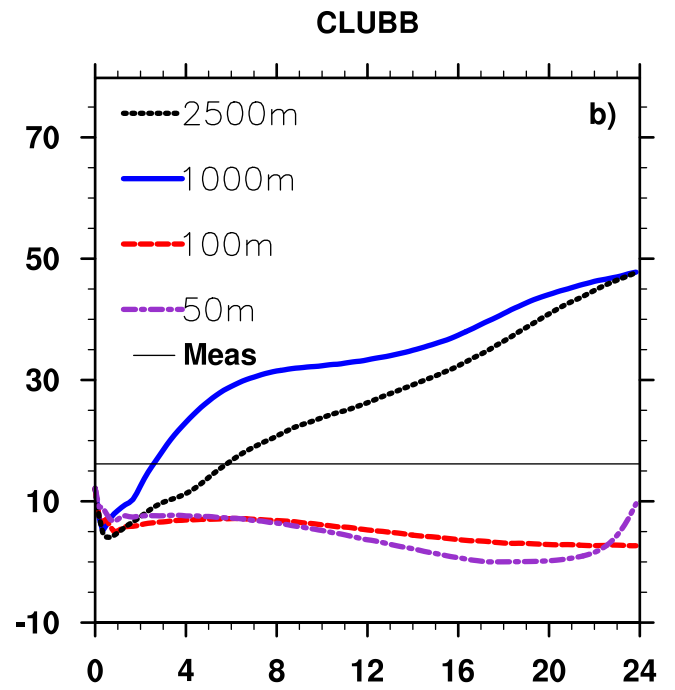
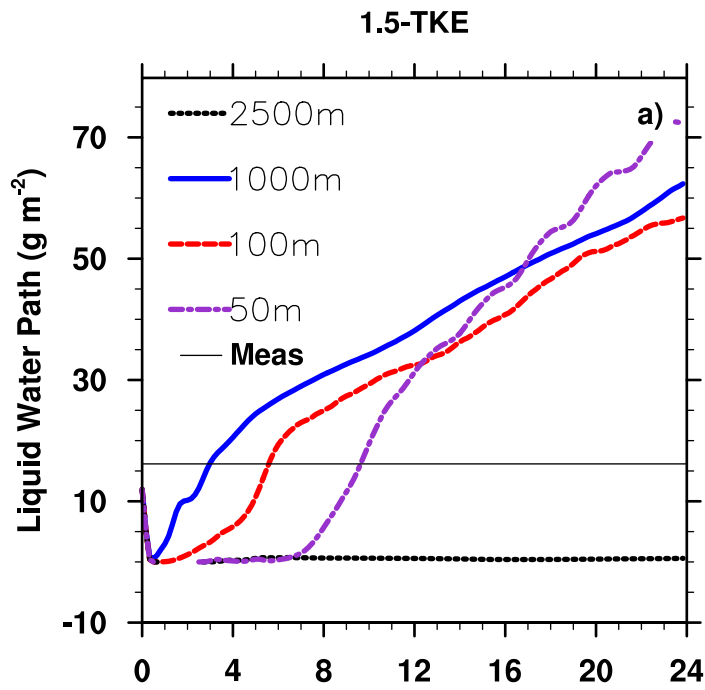
Downwelling Longwave Flux at Surface (W m^{-2})

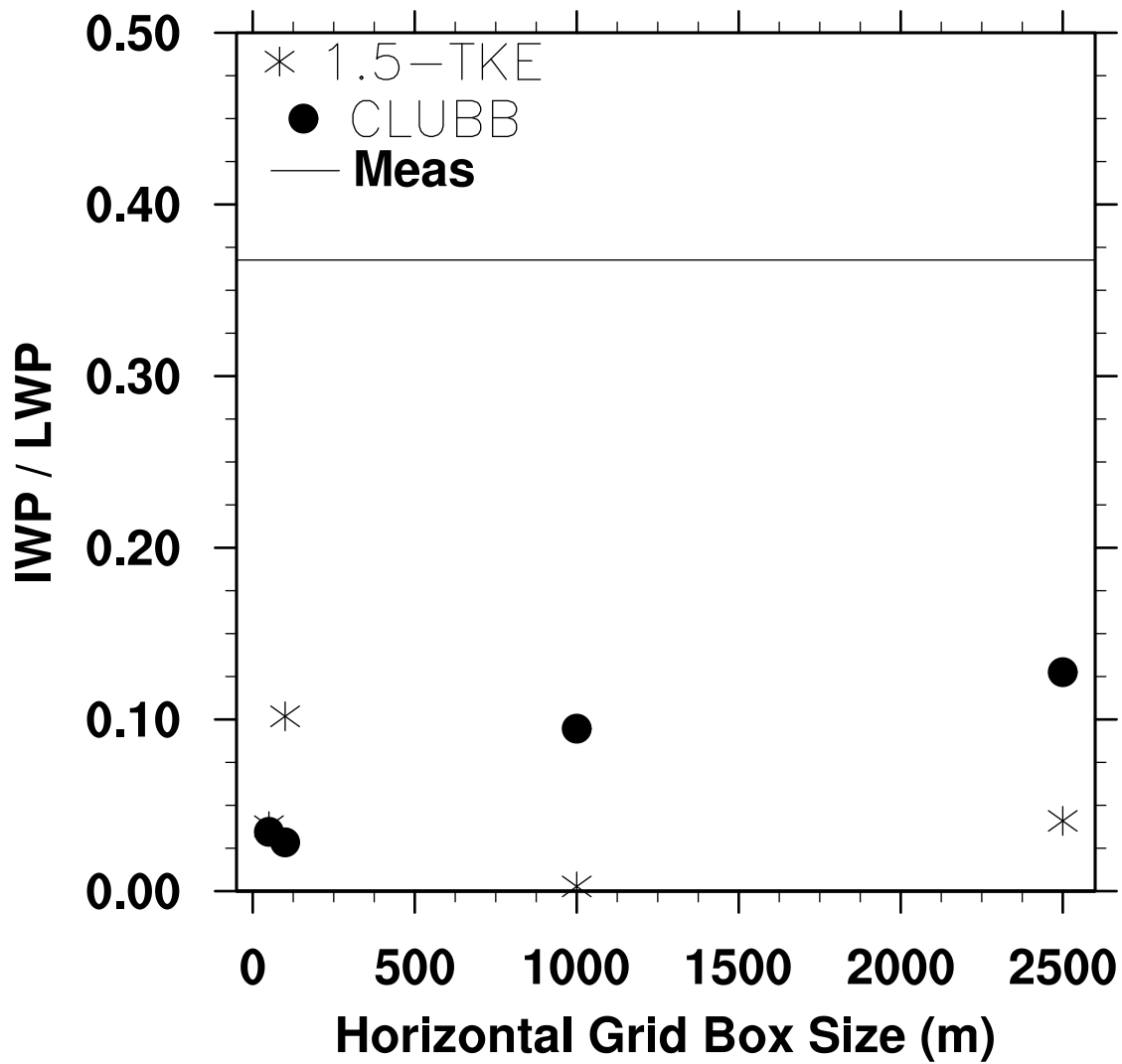




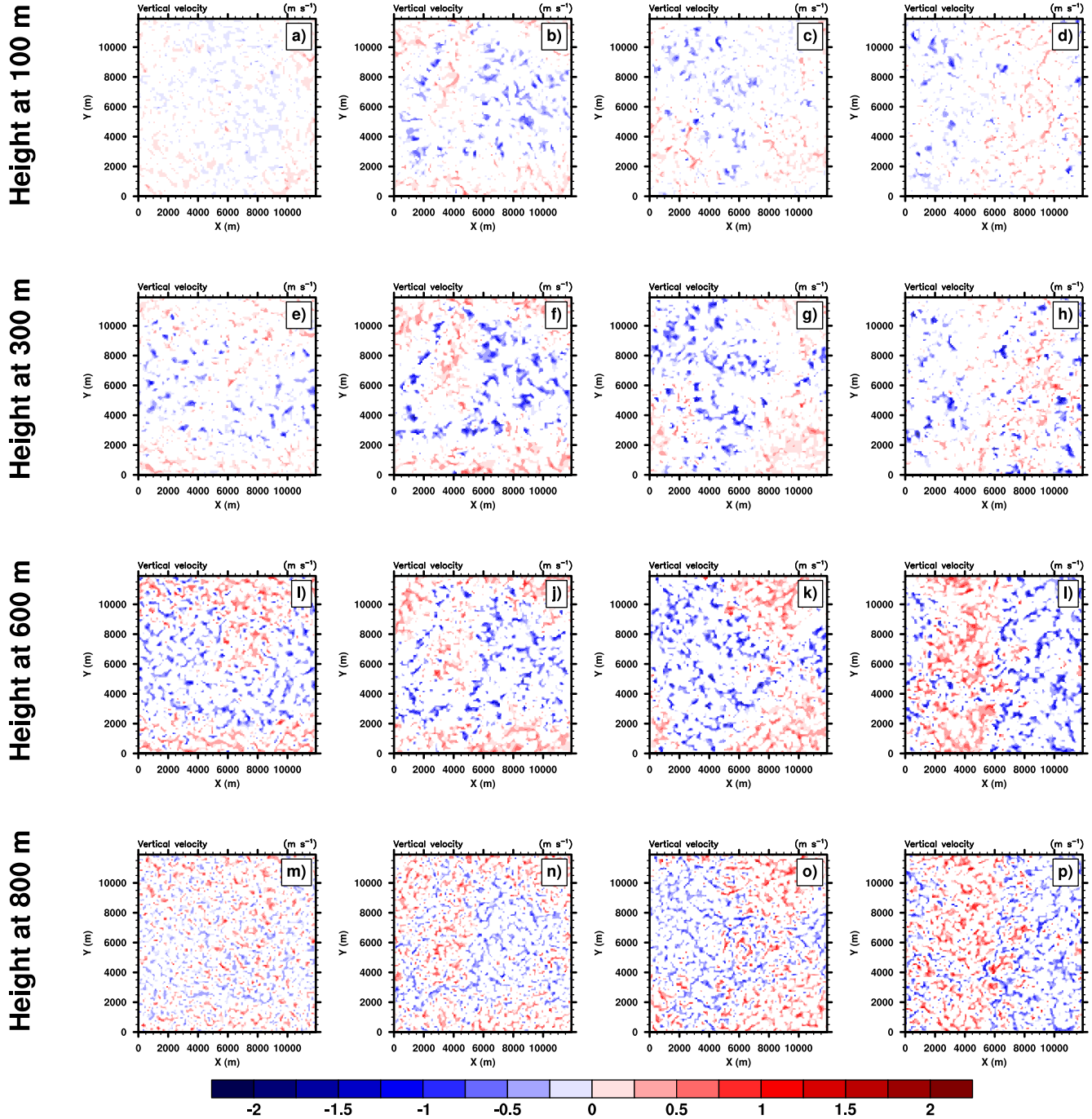




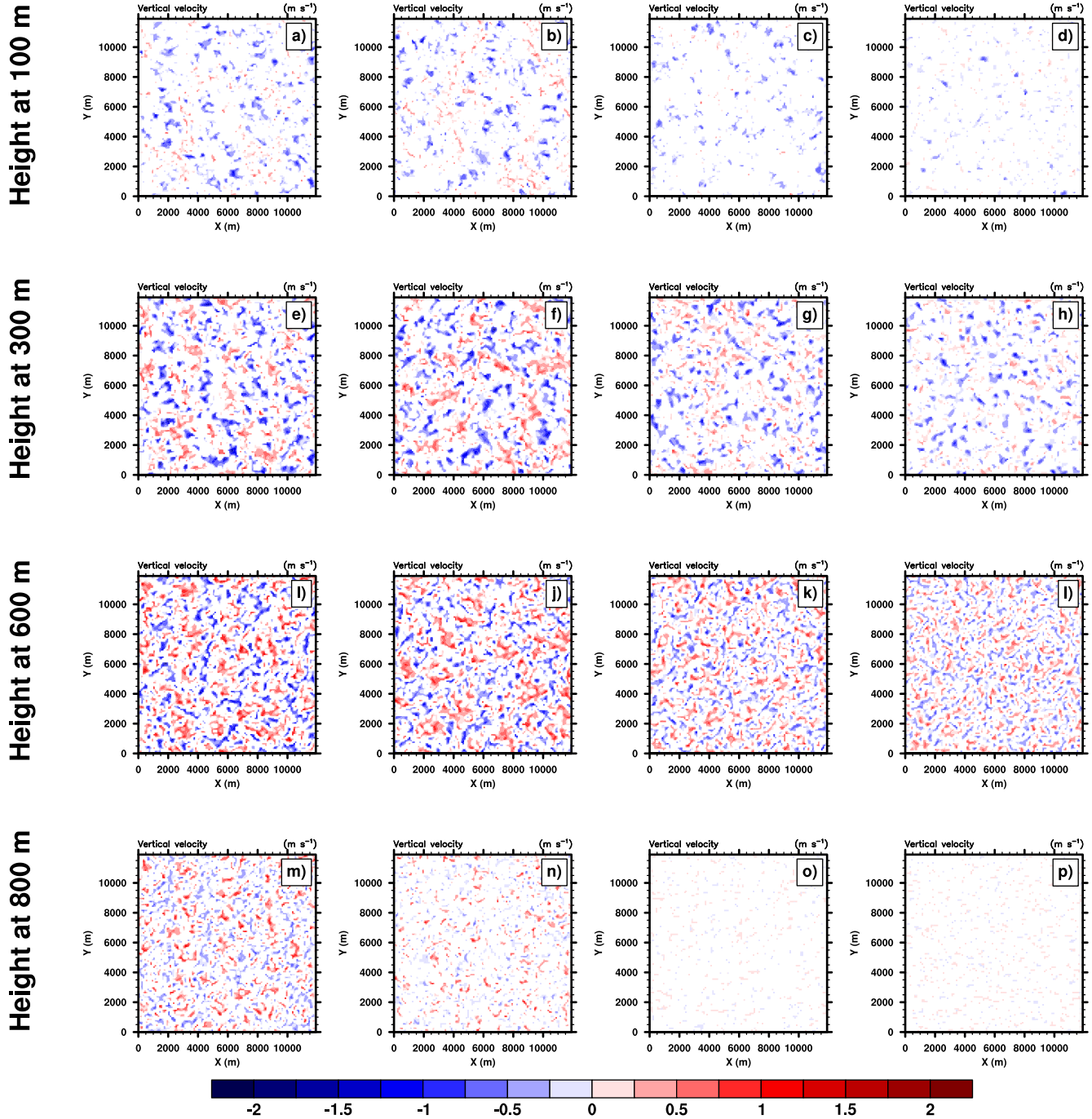


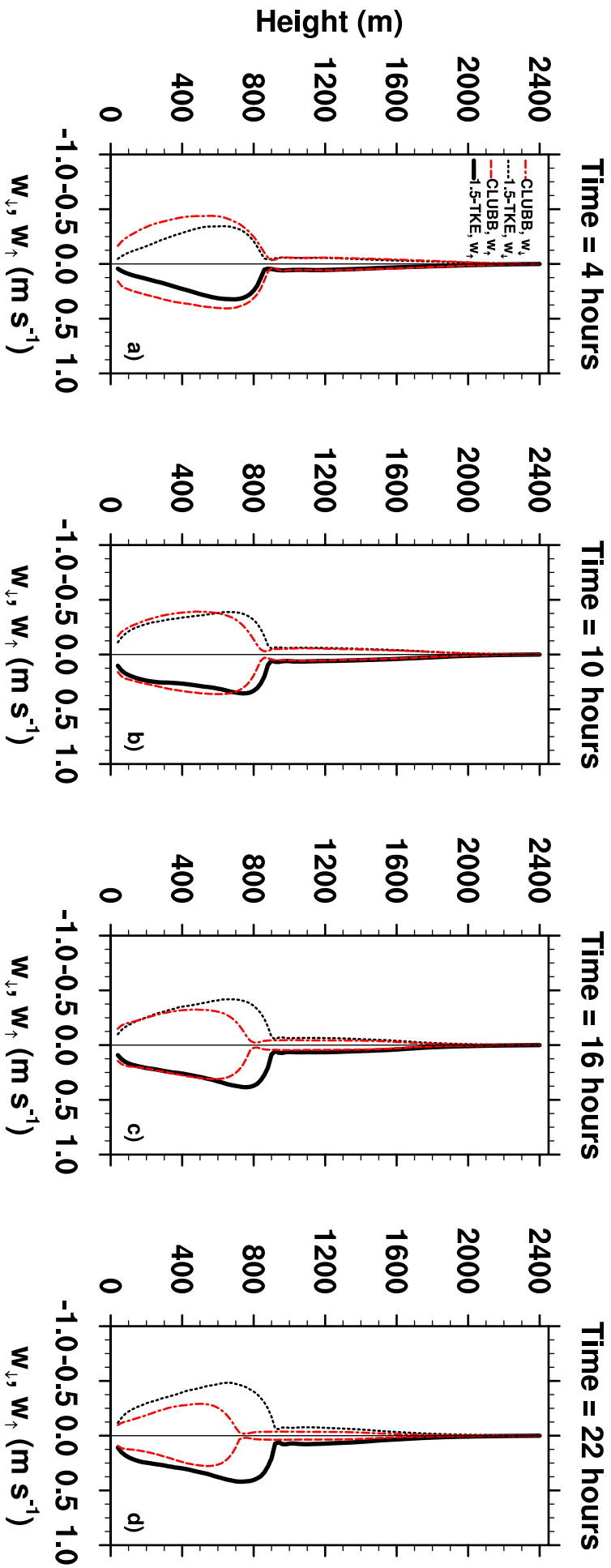


Time = 4 hours Time = 10 hours Time = 16 hours Time = 22 hours



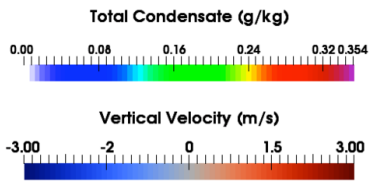
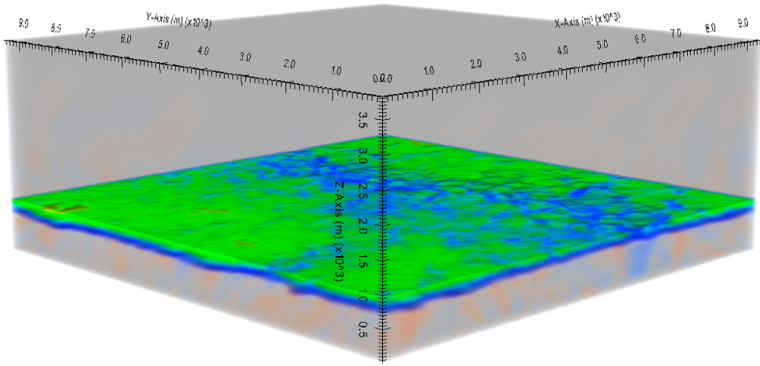
Time = 4 hours Time = 10 hours Time = 16 hours Time = 22 hours





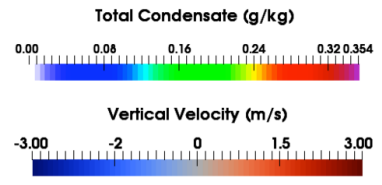
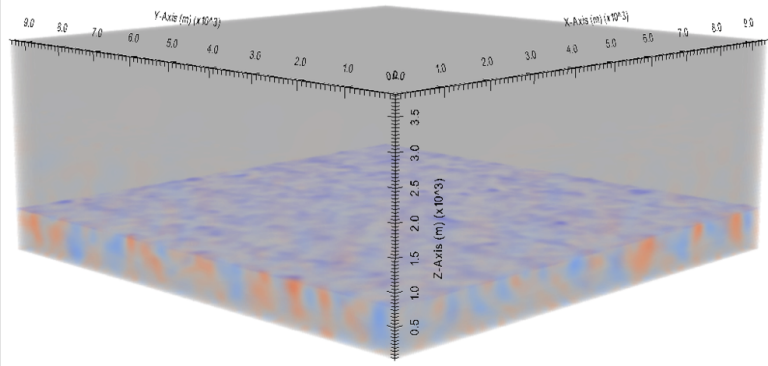
ript

1.5-TKE



Time: 118.000000

CLUBB

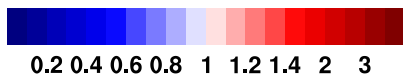
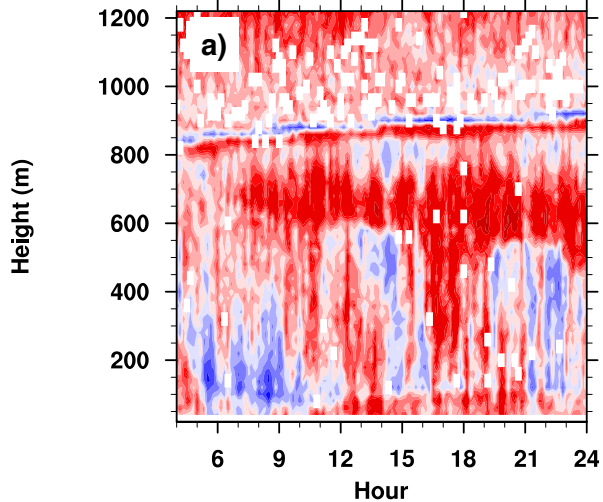


Time: 118.000000

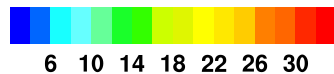
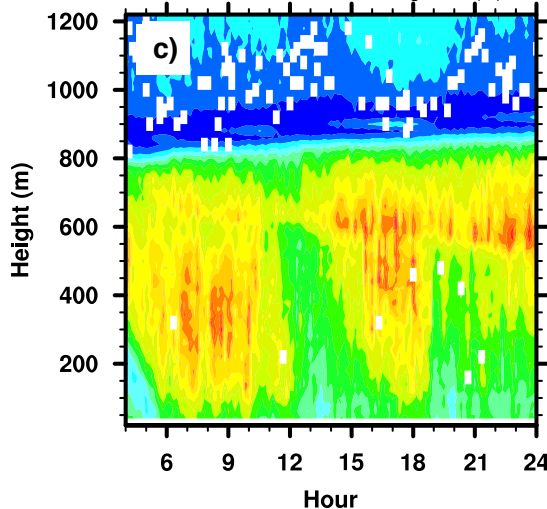
2016JD026055-f15-z-.png

Au

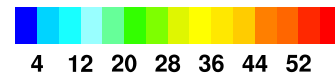
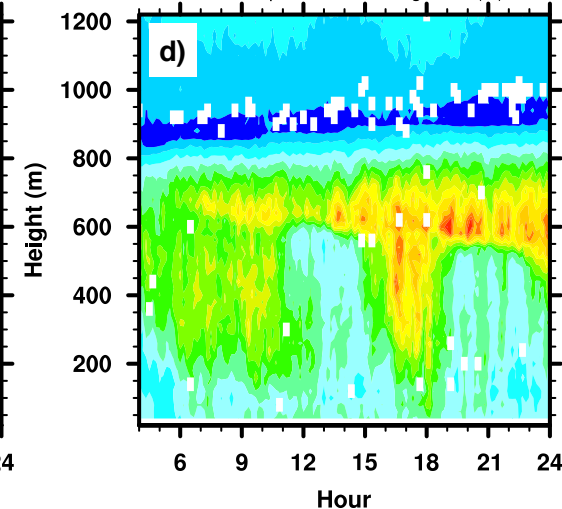
1.5-TKE: Ratio of average of updraft to downdraft core size



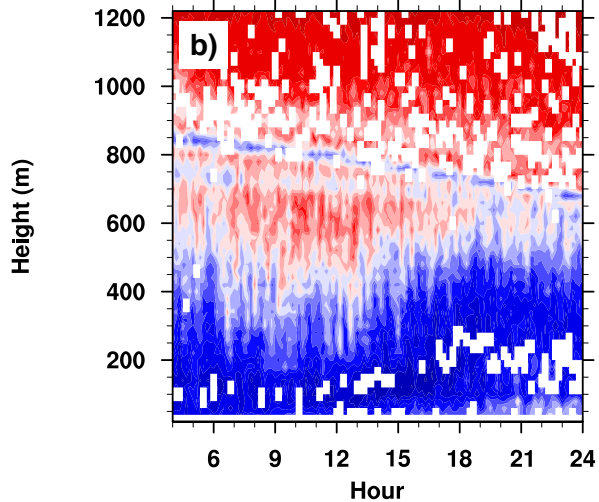
1.5-TKE: downdraft core average size ($\times 10^4 \text{ m}^2$)



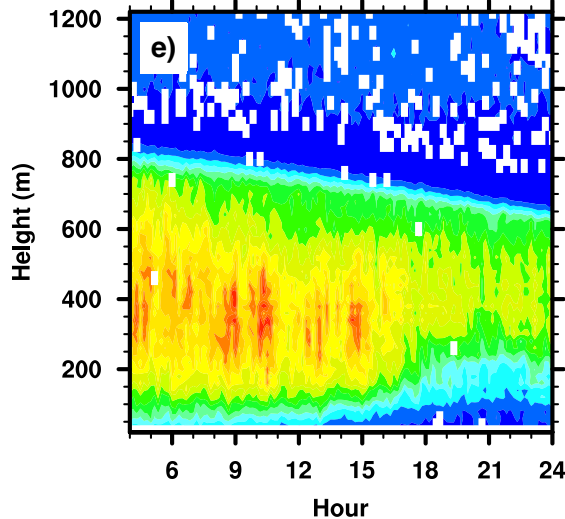
1.5-TKE: updraft core average size ($\times 10^4 \text{ m}^2$)



CLUBB: Ratio of average of updraft to downdraft core size



CLUBB: downdraft core average size ($\times 10^4 \text{ m}^2$)



CLUBB: updraft core average size ($\times 10^4 \text{ m}^2$)

